Chapter 2

Methods for estimating glacier mass balance

Glaciers form when the local climate is both cold and moist enough to deposit ice and when the accumulation of ice exceeds its loss over a time span longer than a few years. They occur in many different forms and locations. The majority of the world's glacial ice is found in polar to subpolar regions, however favourable conditions also occur at high altitudes worldwide. They range in size from the large ice sheets at the polar regions that are thousands of kilometres wide, to valley glaciers often only a few hundred meters long. Glaciers can be categorized according to their size or location; glaciers categorized by size include ice fields, ice caps, and ice sheets; glaciers categorized by location include alpine-, valley-, and piedmont glaciers. In this study the latter three types of glaciers, together with ice caps, are referred to as *mountain glaciers*. Independent glaciers and ice caps around the ice sheets of Antarctica and Greenland are discussed, but generally not included here unless stated otherwise.

In the first half of the 19^{th} century Louis Agassiz, Thomson, Forbes, Tyndall, and others began observing the movements and flow-behaviour of existing glaciers. Additionally, studies of previously glaciated terranes allowed the first reconstructions of past ice ages. Systematic measurements of glacier flow began around 1830, in particular to establish the spatial distribution of movements on a glacier. During the rest of the 19^{th} century short and sporadic measurements of volume changes were carried out, mostly in the European Alps (e.g. Finsterwalder and Schnuck, 1887; Finsterwalder, 1897).

In 1894, the International Glacier Commission (Commission Internationale des

Glaciers, CIG) was created, with the task of 'inciting and spreading the studies of changes in the sizes of glaciers' (Radok, 1997, p. 131). A series of annual CIG reports entitled "Les variations périodiques des glaciers" recorded the results of glacier surveys and historical data from different parts of the world. This series started with a memorandum by Forel (1895) which established technical concepts and terms to provide a foundation for a long term research programme about glacier variations and systematics. This early work had already acknowledged the effect of climate variations on glaciers. In 1924 the International Union of Geodesy and Geophysics (IUGG) created the "International Section of Hydrology", soon to become the International Association of Scientific Hydrology (IASH). The CIG was incorporated into the IASH in 1927, which created a Glacier Commission. After World War II the IASH Commission on Glaciers and Snow reappeared under its new name, the International Commission on Snow and Ice (ICSI; Radok, 1997). A report from a ICSI sub-commitee on glacier variations created the basis for a renewed monitoring of world-wide changes of glaciers as well as polar ice sheets. In 1962, the Permanent Service for the Fluctuations of Glaciers (PSFG) and a World Glacier Inventory were set up. In 1985 the PSFG merged with the World Glacier Inventory's "Temproary Technical Secretariat" to become the World Glacier Monitoring Service (WGMS; Radok, 1997). At present, the WGMS had published seven volumes on the "Fluctuations of Glaciers" and also completed eight series of the "Glacier Mass Balance Bulletins". The WGMS operates the "Global Terrestrial Network for Glaciers" which is an integrative approach 'based on a combination of *in situ*, remote and numerical modelling components and consists of observations at several levels which link detailed process studies at one extreme with global coverage by satellite imagery and digital terrain information at the other' (Haeberli, 2006, p. 424). Already in 1936 at the General Assembly of IUGG a proposal for the creation of a separate "Association of Cryology" was put forward, but without success (Jones, 2008). Only in 1999 the first steps were coordinated for a transition from a Commission to Association. Finally, in 2007 the International Association of Cryospheric Sciences (IACS) was accepted as the eighth Association of IUGG (Jones, 2008).

The historical overview above indicates that from the late 19^{th} century, the causes and consequences of glacier fluctuations have become of growing interest for various reasons, both on a scientific and economic level. For example, exploitation of glacial runoff for hydropower generation (e.g. in Switzerland; Schaefli et al., 2007) and irrigation (e.g. in the Andes) has been investigated, providing an economic benefit in areas surrounded by glaciers. Also, freshwater supply in many regions

is controlled by the run-off from mountain glaciers. Thus, their growth and shrinkage can have dramatic impact on the economic, social, and cultural activities in regions close to mountains. However, other studies have focused on the hazards associated with glacial blocking, glacial floods, and ice/snow avalanches, and the social impact that these natural events can entail (e.g. Richardson and Reynolds, 2000). Alternatively, studies on the potential contribution to global and local sea-level changes from the melting of continental ice masses are relevant to recent scientific discussions on global warming and can be used as a proxy to study past climate change in an attempt to predict future patterns (e.g. IPCC, 2001, 2007b, and references therein).

In 1920, Ahlmann initiated investigations on the glacier response (retreat/advance) to changes in climate focusing on glaciers in Scandinavia, Spitsbergen, Iceland, and Greenland (Ahlmann, 1935). From a global analysis of volume changes from 1850 onwards, Thorarinsson (1940) concluded that the present glacier shrinkage is a universal phenomenon, and that the global recession of glaciers has taken place in several stages with ever increasing intensity, interrupted by intervals of stagnation. Studies over the last few decades by M. F. Meier, R. J. Braithwaite, J. Oerlemans, M. Dyurgerov, S. C. B. Raper, to name only a few, all indicate that mountain glaciers are very sensitive to climate variations, hence they serve as important indicators of such change.

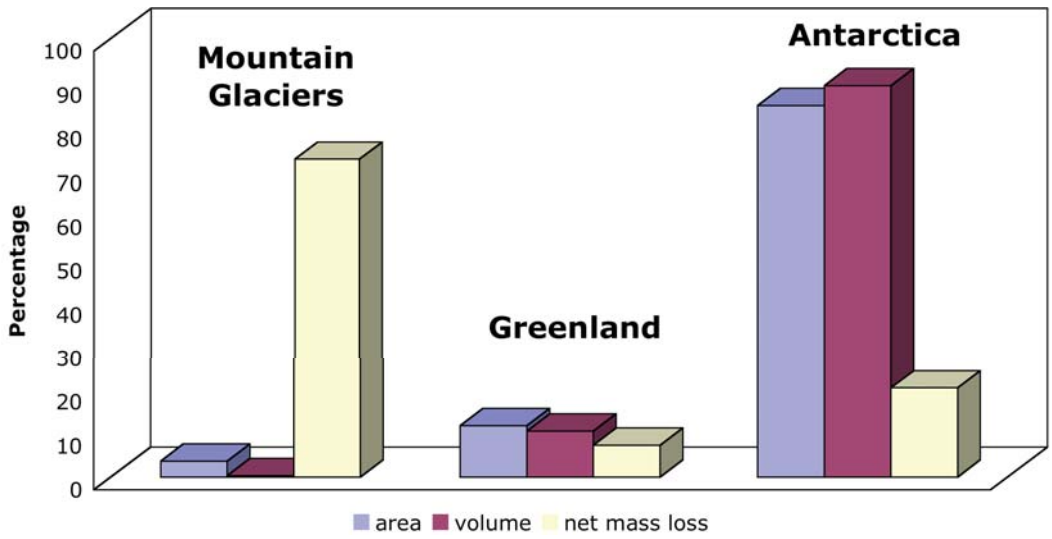

Figure 2.1: Comparison of area, ice volume, and net mass loss (and hence the projected contribution to global sea-level rise) for the period 1961-2003 between ice masses of *Mountain Glaciers*, *Greenland*, and *Antarctica* according to the IPCC (2007b) report. It illustrates that the contribution to global sea-level rise from mountain glaciers is significantly larger than from Antarctica and Greenland together.

At present, the global glacier area is relatively well constrained, with only minor uncertainties, such as temporal and spatial gaps. In contrast, global glacier volume is more difficult to determine. According to the IPCC (2001) report, melting of all mountain glaciers including independent (so-called 'local') glaciers and ice caps around the Antarctic and Greenland ice sheets would raise sea level by 0.5±0.10 m. The Antarctic and Greenland ice sheets store water equivalent to approximately 60 and 7 m of global sea-level rise, respectively. The IPCC (2007b) report updated these numbers to 0.15-0.37 m potential sea-level rise from glaciers and ice caps (excluding those around the Antarctic and Greenland ice sheets; Ohmura, 2004; Dyurgerov and Meier, 2005) and 56.6 and 7.3 m sea-level rise from the Antarctic and Greenland ice sheets (Lythe et al., 2001; Bamber et al., 2001). Although the amount of ice stored in mountain glaciers is much smaller than in the Greenland or Antarctic ice sheet, they are considerably more dynamic on short time scales. Recent past, present, and near future changes in mountain glacier volume are therefore important contributors to global sea-level rise on decadal and centennial time scales (Figure 2.1). This thesis investigates recent past and future mountain deglaciation and its contribution to global and regional sea-level changes.

The determination of changes in mountain glaciers relies on various methods that have been developed in the past few decades. In the following section, I define the key parameter to this study, the *glacier mass balance*, and give an overview of *observational* methods used for its determination. Section 2.2 discusses the basics of a *numerical* approach used to model ice-volume changes of mountain glacier that are based on meteorological data. Section 2.3 gives a description of the global data sets used in the numerical modelling.

2.1 Observations of glacier mass balance

Changes in mountain glaciers can be determined in a number of different ways, such as measurements of changes in surface area, surface elevation, ice volume, ice mass, or in melting rates. In order to determine the sea-level response to volume changes in mountain glaciers, variations in ice mass of the glaciers with time are required. The term *glacier mass balance* $\boldsymbol{B}$ is used to describe the change in ice-mass and is usually expressed in kg m^{-2} or as the equivalent volume of liquid water in m^3. Throughout this thesis, the latter expression (volume-unit) is used and where required the mass-units were converted to volume-units by using the densities of water and ice at 0°C of 1 and 0.917 g cm^{-3}, respectively. Note that

changing the temperature by 40°C results in a variation of both densities by less than 1% and hence this uncertainty is negligible. There are two main contributions to the mass balance of a glacier (Glossary of Geology, 2005):

- ➢ mass loss (ablation) from all processes by which snow and ice are lost from the glacier, such as melting, sublimation (ice changes into water vapour without first becoming liquid), wind erosion, avalanches, and ice flow into the sea
- ➢ mass gain (accumulation) from all processes that add snow or ice to a glacier, such as snow fall, condensation, avalanching, wind transport, and freezing of liquid water

The observed mass balance B of mountain glaciers is defined as the difference between accumulation and ablation. If $B > 0$ the glacier is increasing in its mass, if $B < 0$ the mass of the glacier is decreasing. The *specific-* or *surface mass balance* of a glacier is the net amount of ice mass gain or loss at the point on the surface of a glacier, usually expressed in meter. Mass balance not only varies with altitude but also has horizontal differences. However, these latter variations are far less pronounced. The *mean specific mass balance* of a glacier (also expressed in meter) is the specific mass balance averaged over the entire glacier. A *mass balance rate* (e.g. annual) is the net gain or loss of mass of a glacier each year and hence has the unit m^3 $year^{-1}$ of water. In the literature, the terms balance (m^3 of water) and balance rate (m^3 $year^{-1}$ of water) are not always used consistently.

Glacier mass balance is monitored at numerous sites worldwide, but the presently available data are strongly biased to western Europe, North America, and the former USSR and are further biased to glaciers with small areal extent. Measurements of glacier mass balance can be achieved directly from *in situ* observations and indirectly using geodetic methods.

- **Direct *in situ* measurements**
  In order to determine the mass balance in the accumulation zone, snowpack depth is measured using probing[1], snowpits[2], or crevasse stratigraphy[3]. In

[1]Probing is done by driving a probe through the relatively soft snowpack from the previous winter. The snow-firn that survived the previous summer or blue ice under that snow is much harder and cannot be penetrated.

[2]Pits are dug to measure the net balance in the accumulation zone. The previous summer surface is usually marked by a layer of dirt in the firn or by sudden change in density, hardness or grain size.

[3]Annual snowlayer thickness is visible much like tree rings, providing a two dimensional measurement of snowpack thickness and thus is more accurate than point measurements from probing of snowpits. However, only vertically walled crevasses can be used.

the ablation zone, ablation measurements are made using stakes[4] inserted vertically into the glacier, either at the end of the previous melt season or the beginning of the current one. Without complete coverage, measurements of glacier mass balance are difficult to obtain and are subject to significant uncertainty. Specific mass balances for glaciers around the globe are poorly known. Observational constraints on mass balances for the past century are available for only a few glaciers mainly in the northern hemisphere (e.g. Pelto, 1996; Kuhn et al., 1999; Trabant and March, 1999). These measurements of glacier mass balances reach back to the mid 20^{th} century, but in most cases with high variability in observation intervals. Continuous mass balance records longer than 20 years exist for about 40 glaciers worldwide; more than 100 glaciers have records of 1 to 5 years (Dyurgerov and Meier, 1997a). Given the total number of glaciers around the world of more than 160,000 (Church et al., 2001), the available mass balance observations represent only a very small fraction of the total. Consequently, direct estimates for the total mass balance of the world's mountain glaciers are poor.

- **Indirect geodetic methods**
  Geodetic methods are an indirect approach used for the determination of the mass balance of a glacier. Maps of a glacier made at two different times can be compared and the difference in surface elevation observed can be used to determine the changes in mass balance with time. Two commonly used approaches are given below (Baltsavias, 1999):

  ➢ Aerial mapping or photogrammetry:
  Past glacier surface profiles (i.e. images used to make topographical maps and digital elevation models) can be compared to more recent images to estimate mass balances. By comparing results for different epochs and by using average densities for firn and ice, the change in volume of the glacier can be determined. Problems with photogrammetry include the poor contrast of snow-covered glacier surfaces and the necessity for cloud-free conditions over almost the entire image. Furthermore, field work and analysis are time-consuming. Another limitation to photogrammetric methods is that ground control points can be difficult to identify and consequently can result in elevation errors. Keutterling and Thomas (2006) conclude that for the case study of the Gepatschferner (Austria) the average vertical error in the digitised maps

[4]Ablation measurements are done by emplacing stakes into the glacier and measuring the change in height above the glacier surface on several occasions.

from aerial surveys are of the order of ±1 m in level terrain but increases to ±6 m for a slope of 60°.

➢ Airborne laser altimetry:
Variations in glaciers are often manifested in the advance and retreat of their termini. However, volume changes of mountain glaciers and especially of ice caps can also occur with little indication along the perimeter. Under these conditions, the laser altimetry system becomes a useful tool in detecting the changes in ice masses. This method provides a measurement of the elevation of a glacier along a specific path, e.g. the glacier centreline. The difference of two such measurements is the change in thickness, which provides an estimate of the mean mass balance change over the time interval between the measurements. Such elevation surveys provide the most direct large-scale means of examining the state of glaciers. In flat and snow covered parts of a glacier, laser scanning methods can reach an accuracy of 0.2 m in the vertical direction (Geist and Stötter, 2002). This accuracy is mainly affected by uncertainties in the laser range and the GPS position of the aircraft (Kennett and Eiken, 1997). Furthermore, the accuracy of surface elevation is reduced with increasing slope of the surface and also over crevassed areas. Geist and Stötter (2002) estimated that for the Unteraarferner (Switzerland), laser scanning methods produce surface elevation changes with an accuracy of 0.5-0.7 m. An additional possible uncertainty factor results from the signals intensity which changes significantly between different glacier surface classes (i.e. ice, snow, firn, and surface irregularities). Thus, this method is only useful for measuring mass balance over a relatively long time span in which changes are expected to have exceeded the mean accuracy (van der Veen, 1993).

The advantage of these geodetic methods is that they provide an independent check of *in situ* mass balance work, by comparing the cumulative changes over ten or more years on glaciers where the change is significantly larger than the measurement uncertainty. However, mass balance measurements determined by geodetic methods are confined to the past few decades and have only been undertaken on a relatively limited number of glaciers.

2.2 Numerical methods

Direct measurements of glacier mass balance provide many important insights into the changes in ice volume with time for individual glaciers. However, extrapolating from these observational constraints made in a few regions to make global estimates of glacier mass balance can lead to considerable uncertainty (Braithwaite, 2006). Hence, an indirect method is preferred here to determine glacier changes. This can be based on detailed evaluation of the surface energy fluxes (*energy-balance models*) or on models using air temperature as a sole index of melting rates (*temperature-index* or *degree-day models*). The latter (e.g. Rango and Martinec, 1995; Hock, 2003, and references therein) assumes an empirical relationship between melt and air temperature based on a strong and frequently observed correlation between these quantities. In contrast, in the energy-balance model (e.g. Oerlemans, 2001; Hock, 2005) the mechanism of the energy fluxes to and from the glacier is developed using processes at the glacier-atmosphere interface such as:

- turbulent exchange of sensible and latent heat,
- ice heat flux,
- sensible heat flux of rain,
- solar radiation,
- longwave radiation, and
- albedo.

Turbulent heat fluxes are primarily dependent on temperature- and moisture gradients and wind speed. Solar and longwave radiation is dependent on cloudiness. Albedo, in turn, is determined by factors related to the surface itself, such as grain size, water content, impurity content, surface roughness, crystal orientation, and structure, as well as whether the sunlight is diffuse or direct. Processes within the thermal structure in the upper layer of the glacier, including

- molecular conduction,
- thermal convection by air motion,
- convection of water vapour, and
- flow of melt water,

result in much smaller fluxes than those between glacier surface and atmosphere, except for the flow of melt water. The relative importance of the components of the energy balance model depend strongly on weather conditions, hence their relative contributions may change during the accumulation and melt season. The

total melt is influenced by all components of the energy-balance model, hence many attempts have been made to incorporate more variables. This also means that this method becomes computationally very complex. With computers ready to perform complex computations, there is seemingly no obstacle to replace a simple method of computing snowmelt with a more sophisticated one. Energy-balance processes are believed to be well understood and are amenable to modelling, with the notable exception of maritime ablation through iceberg calving and basal melting beneath ice shelves. At sites where extensive meteorological and snow surveying data are available, successful energy-balance models have been developed. However, this is valid on point scales only. Unfortunately, detailed energy-balance data are not available for most ice masses, nor are they well predicted by global- or regional climate models. This has led to the development of reduced models for snow and ice melt, in particular parameterizing melt rates as a function of temperature changes. Temperature is generally considered to be the most readily available data quantity and is reasonably easy to extrapolate and forecast. Hence, these simplified parameterizations of snow and ice melt permit distributed modelling in a region where ground observations are scarce. However, the temperature-index models involve a simplification of complex processes that are more properly described by the energy-balance method. Nevertheless, temperature-index models often complement the energy-balance models, due to the generally high correlation between temperature and various components of the energy-balance model.

Concluding, changes in glaciers are strongly related to climate parameters such as temperature and precipitation that control the accumulation and melting of snow and ice. Conversely, change in mass balance is the most sensitive climate indicator on a glacier. In the case where no direct measurements of glacier mass balances are available, the ice-volume change ΔV of a mountain glacier can be approximated with the following equation:

$$\Delta V = A\, \Delta T\, \Psi \tag{2.1}$$

where A is the area of the glacier, ΔT represents the temperature change over time, and Ψ is the sensitivity of the mean specific glacier mass balance rate to temperature changes, i.e. Ψ is a function of temperature change and hence $\Psi = \Psi(\Delta T)$. In other words, a mass balance sensitivity is the derivative of the mass balance with respect to a climate parameter that affects it, e.g. mass balance rate to temperature changes $\Psi(\Delta T)$ as in above. With both methods mentioned above (temperature-index and energy-balance models) the mass balance sensitivity can

be determined (as discussed for example in Braithwaite and Zhang, 1999a), and has been carried out for a number of individual glaciers. The result of Equation 2.1 gives the change in ice volume ΔV for the particular glacier for the period the temperature change is recorded. The key parameters for this method are:

- the area of the glacier,
- the sensitivity of glacier mass balance rate to temperature changes, and
- the temperature changes over time.

With available data sets for these parameters, a more detailed model for ice-volume changes over a time period can be established. In particular, a separation between mass balance sensitivities to summer and non-summer temperature changes is made that accounts for the seasonal variations in temperature. According to Gregory and Oerlemans (1998) using the annual temperature changes at the glacier overestimates the ice-volume change. Hence, the seasonality of temperature changes and mass balance sensitivities is considered here and the resulting equation of ice-volume changes for a glacier k over the time period t is:

$$\Delta V_k(t) = A_k \sum_{t_0}^{t_1} \{\Delta T_{s,k}\, \Psi_k(\Delta T_s) \; + \; \Delta T_{ns,k}\, \Psi_k(\Delta T_{ns})\} \tag{2.2}$$

where the subscripts s and ns denote summer and non-summer periods.

The relationship (2.2) assumes that the temperature changes $\Delta T_{s,k}$ and $\Delta T_{ns,k}$ are relative to a time period in which the glacier and the climate were in equilibrium, i.e. it implicitly treats the initial glacier distribution as if it is in an equilibrium state with the reference climate. This is certainly not the case since glaciers rarely reach steady state in their response to ever-changing climate (Jóhannesson et al., 1989). Observations show that glaciers in recent years may still be responding to earlier climate fluctuations on larger than annual- or decadal time scales such that the equilibrium may never be realised. The following studies show the evidence for this imbalance and also one simple way to quantify it.

- **Kruss (1983)** uses 100 years of terminus records at Lewis glacier, Mount Kenya, to infer a climatic signal. During the last quarter of the 19^{th} century, available instrumental evidence lend strong evidence for a precipitation decrease, but little support to a temperature increase in the tropics. However, of the three scenarios Kruss (1983) investigated one is based on temperature and albedo changes and he projected from the observed terminus record a

possible warming of 0.4±0.25 K between the early 1880s and the turn of the 19^{th} century.

- **Oerlemans (1992)** analysed mass balance characteristics on three glaciers in southern Norway: Alfotbreen, Hellstugubreen, and Nigardsbreen. Their established energy-balance model successfully simulates the observed mass balance profiles and hence can be used for climate sensitivity studies. Sensitivity studies assessing the effect on the glacier equilibrium-line altitude[5] to changes in temperature show that Alfotbreen is by far the most sensitive and Hellstugubreen is the least sensitive glacier. Alfotbreen, an extreme maritime glacier, is almost twice as sensitive as Hellstugubreen, a continental glacier. The variability in the equilibrium-line altitude is less than that of the specific mass balance which is a consequence of the changing mass balance gradient. Each of the glaciers show varying degrees of sensitivity to changes in precipitation rates. A 20% change in precipitation has roughly the same effect on the equilibrium-line altitude as a 1 K temperature change. Coupling the mass-balance model to a flow model to simulate mass balance profiles (i.e. specific mass balance as a function of surface elevation) shows that at the Nigardsbreen, a retreat of more than 6 km is predicted for a 1 K temperature increase. The glacier advances 3 km in response to a 1 K cooling. A drop of 10% in precipitation results in a 4 km retreat.
  From these sensitivity studies, in particular from the projected retreat of the glacier (which matches the observations) in response to temperature changes, the relationship of a retreat of 6 m per year for an increase in temperature of 0.001 K can be determined. This relationship is only an approximation as changes in glacier termini are also dependent on other factors such as the glacier geometry (e.g. Oerlemans, 1997). However, the above relationship can then be used to quantitatively determine the imbalance of the glacier and climate state. This assumes that the imbalance is entirely determined by the temperature change within the considered period.

- **Greuell (1992)** studied the historical length variations of the Hintereisferner in Austria. Observed length variations at Hintereisferner began in 1847 and in 1855 the maximum observed length was reached. Since then the glacier retreated continuously except for the one period of advance between 1917 and 1922. Historical length variations of Hintereisferner are shown in Figure

[5]The term equilibrium-line altitude is defined as the elevation at which the accumulation zone is separated by the ablation zone. By definition, the specific mass balance at the equilibrium line is zero.

3 in Greuell (1992). A retreat of about 600 m between 1860 and 1890 was measured. Assuming the same response in glacier length to temperature changes as in Oerlemans (1992) of 6 m year^{-1} retreat per temperature increase of 0.001 K, results in a 0.10 K temperature increase between 1860 and 1890.

- **Stroeven et al. (1989)** developed a numerical ice-flow model and simulated the historic front variations of the Rhône glacier in Switzerland. Front positions of the glacier since 1602 are available. Stroeven et al. (1989) note that the glacier has shown (more or less) a steady retreat since 1856. From Figure 2 in Stroeven et al. (1989) a retreat of around 900 m over the period from 1860 to 1890 can be measured. Using the relationship between variations in glacier lengths and temperature developed by Oerlemans (1992) translates this observed retreat of the glacier into an increase in temperature of 0.15 K over the period from 1860 to 1890.

- **Huybrechts et al. (1989)** developed a numerical glacier model for the mass balance of the d'Argentiere glacier in France in order to study the relation in variations to climatic changes. According to Huybrechts et al. (1989) historical records show that the glacier has been receding

  ➢ slowly and discontinuously from 1883 - 1945: 1.1 m year^{-1} and
  ➢ rapidly and uniformly from 1866 - 1883: 37.1 m year^{-1} and from 1945 - 1967: 21.4 m year^{-1}.

  From Figure 8 in Huybrechts et al. (1989) a change in observed glacier length of around 450 m during 1860 and 1890 can be measured. This interval, with a mean retreat of 15 m year^{-1}, translates to an increase in temperature of 0.075 K for this 30-year period assuming the same relationship of changes in glacier lengths to temperature variations as Oerlemans (1992).

- **Zuo and Oerlemans (1997b)** developed a numerical model to simulate the front variations of the Pasterze glacier in Austria. Over the period from 1860 to 1890 observations of the glacier length show a decrease from about 10.4 km to 10.0 km. This historical retreat of the glacier of 400 m can provide information about climatic variability. In particular, using the relationship of changes in glacier lengths to temperature variations as in Oerlemans (1992) translates the observed retreat at the Pasterze glacier to a temperature increase of 0.07 K for this 30-year period.

As mentioned above, Equation 2.2 requires that the state of the glacier is in equilibrium with the prevailing climate. This is not normally true, but the condition

can be satisfied by introducing a correction parameter Θ (in Kelvin) that reflects the assumption that for a particular period (e.g. 1860-1890) the glacier state is one corresponding with a lower temperature than that prevailing in this period. If the current temperature at a glacier is T_1 but the current glacier extent would be in equilibrium with a temperature T_2, then the parameter Θ is defined as the difference $T_2 - T_1$. However, it needs to be noted here that the front-variations are caused by fluctuations in climate parameters which also occurred some time before the observation. Hence, this response time (e.g. Jóhannesson et al., 1989) is not considered in the above attempt to quantify this imbalance. However, according to Marshall (2006), for alpine glaciers and ice fields (small glacier systems) or those with a rapid climate/dynamic response time, a simulation over many decades would give a reconstruction of present-day ice masses that is reasonably in tune with the historical climate forcing. By introducing the parameter Θ into the model, the final refined equation for ice-volume changes of mountain deglaciation (adopted from Zuo and Oerlemans, 1997b) is:

$$\Delta V_k(t) = A_k \sum_{t_0}^{t_1} \{(\Delta T_{s,k} + \Theta)\, \Psi_k(\Delta T_s) \; + \; (\Delta T_{ns,k} + \Theta)\, \Psi_k(\Delta T_{ns})\} \qquad (2.3)$$

where Θ is positive if the temperature was increasing during the reference period[6]. $\Delta T_{s,k}$ and $\Delta T_{ns,k}$ denote temperature anomalies of summer and non-summer months of a glacier k, each expressed in one annual value. Similarly, $\Psi_k(\Delta T_s)$ and $\Psi_k(\Delta T_{ns})$ are mass balance sensitivities of a glacier k to summer and non-summer temperature changes, respectively. The summation in Equation 2.3 starts with the first year and goes until the last year of available observation, on an annual basis. The result of this equation gives the ice-volume changes in km^3 of equivalent water. Despite the advantage of this approach to determine ice-volume changes on a global scale, the simplifications introduced are substantial, e.g. the need to extrapolate meteorological input data places major limitations on the quality of model simulations. The question of how far the weather station data can predict regional glacier variations is discussed in more detail in the following section.

[6]Zuo and Oerlemans (1997b) introduced a negative Θ for an increase in temperature (because Θ represents a lower temperature than prevailing at the glacier) but then subtracted it from the temperature change ΔT in their equation. This has been modified in this thesis, i.e. in Equation 2.3 the parameter Θ is added to the temperature change ΔT. Hence, the sign of the parameter Θ in this thesis is positive for an increase in temperature.

2.2.1 Micro-climate of mountain glaciers

A boundary layer is defined as that part of the troposphere[7], that is directly influenced by the presence of the Earth's surface, and responds to surface forcing with a time-scale of about an hour or less (Stull, 1997). The boundary layer reaches often an altitude of only a couple of kilometres and the so-called free atmosphere overlies this boundary layer.

In turn, glaciers have their own climate system surrounding them. Chapter 3 in Oerlemans (2001) describes in detail the micro-climate of valley glaciers. This micro-climate is mainly determined by the glacier boundary layer and the processes within it. The glacier boundary layer is part of the atmosphere which is directly influenced by the surface of the glacier (see Figure 2.2). In contrast to the free atmosphere, the glacier boundary layer generally has a distinctive daily circle, i.e. temperature, wind speed, and wind direction that can be very different to the large-scale boundary layer or to the free atmosphere. This is illustrated in Figure 2.3 in a case study showing the atmosphere above the melting Pasterze glacier (Austria). Profiles of observations in temperature, wind direction, and wind speed show significant changes within the first few tens of meters above the glacier surface (glacier boundary layer). The wind profiles in Figure 2.3 show another characteristic change at about 800 m height indicating the change from the large-scale boundary layer to the free atmosphere.

Observations of large-scale climate parameters are more accessible and undertaken more frequently, spatially and temporally, than observations made directly on the glacier. Therefore, it is necessary to couple the micro-climate of the glacier to a larger-scale atmospheric system. A case study of such a relationship is described in Chapter 3.10 in Oerlemans (2001). In this contribution, measurements of climate parameters of the Morteratsch glacier in Switzerland have been compared with observations made at two local weather stations. Samedan, at 1704 m altitude and 12 km away from the Morteratsch glacier, is located in the middle of a wide valley. The second weather station, Corvatsch, is located at the top of a mountain at 3297 m altitude and 9 km west of the glacier. Daily mean temperature for the three locations (Figure 2.4) show high correlations for most of the year. However, Oerlemans (2001) concluded that during winter, the temperature at Samedan is decoupled from that of the glacier. According to the author, this is due to the different geographical settings, i.e. the Samedan station is located in a wide flat

[7]The troposphere extends from the Earth's surface up to an average altitude of 11 km.

valley and hence seems to record different climatic features to the one at the glacier. On the other hand, the correlation between Morteratsch and Corvatsch is very high, suggesting that weather stations at high altitudes can be very valuable for estimating the temperature conditions of nearby glaciers (Oerlemans, 2001).

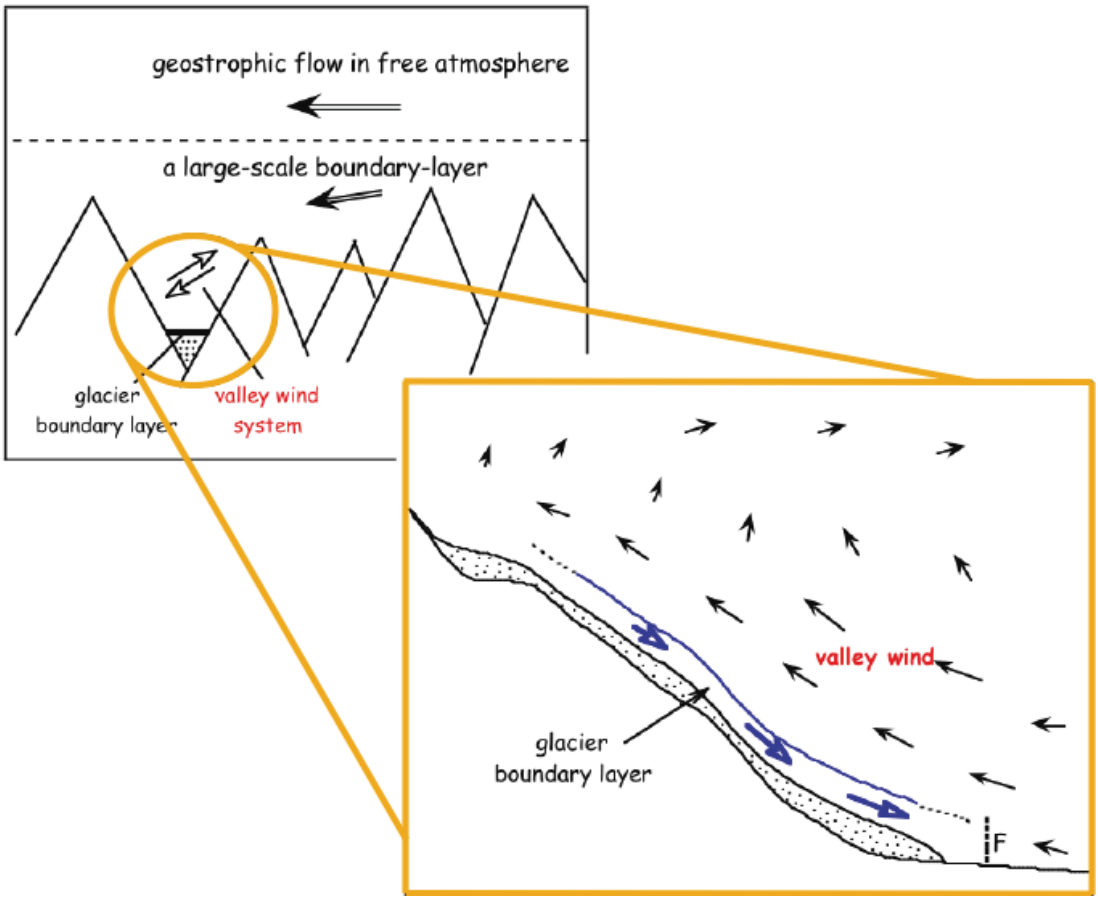

Figure 2.2: Basic structure of atmospheric circulation in a glaciated mountain region (Oerlemans, 2001). The upper left figure illustrates the free atmospheric, the large-scale boundary layer, and the glacier boundary layer. The lower right figure shows in more detail the glacier boundary layer and the prevailing valley wind system above the glacier surface.

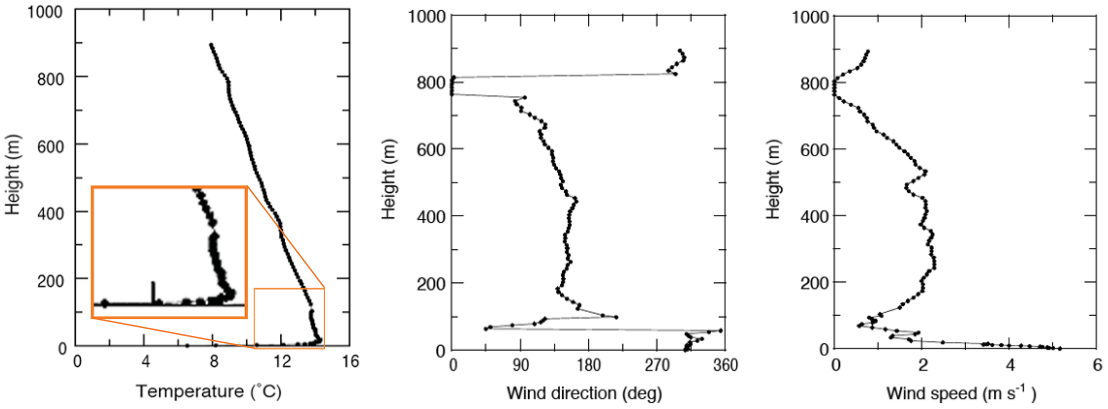

Figure 2.3: Temperature, wind speed, and wind direction measured with a balloon on the 23^{rd} of July 1994 on and above the Pasterze glacier in Austria (Oerlemans, 2001). Significant changes in all three signals can be observed within the first few tens of meters above the glacier surface (glacier boundary layer). The orange box in the left figure highlights the significant change in temperature above the glacier surface caused by turbulent exchange of heat between the atmosphere and the glacier surface. Wind profiles show similar pronounced variations within ∼100 m above the glacier. In addition, a second characteristic change in the wind profiles at about 800 m height indicates the boundary between the large-scale layer and the free atmosphere.

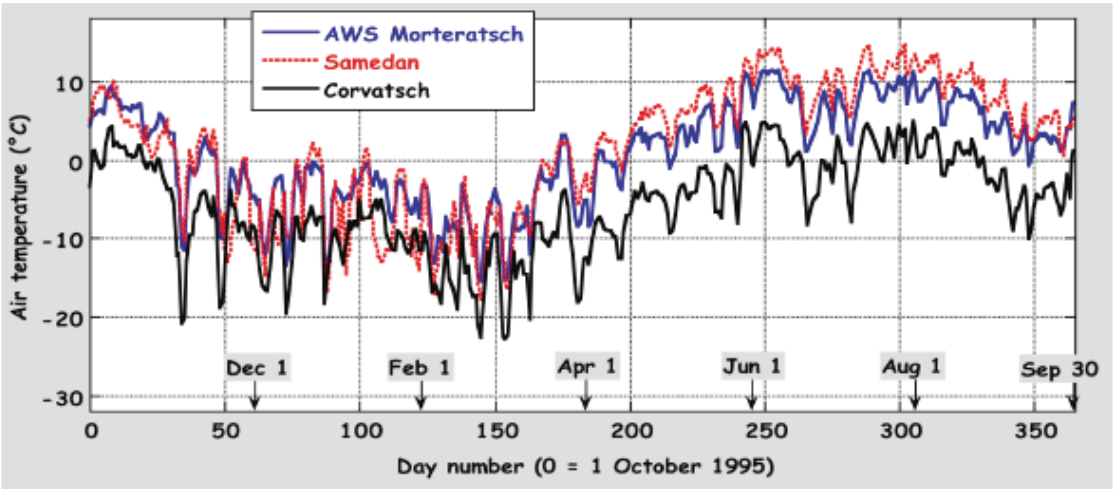

Figure 2.4: Daily mean air temperature for a full year measured on the Morteratsch glacier and the weather stations Samedan and Corvatsch (Oerlemans, 2001).

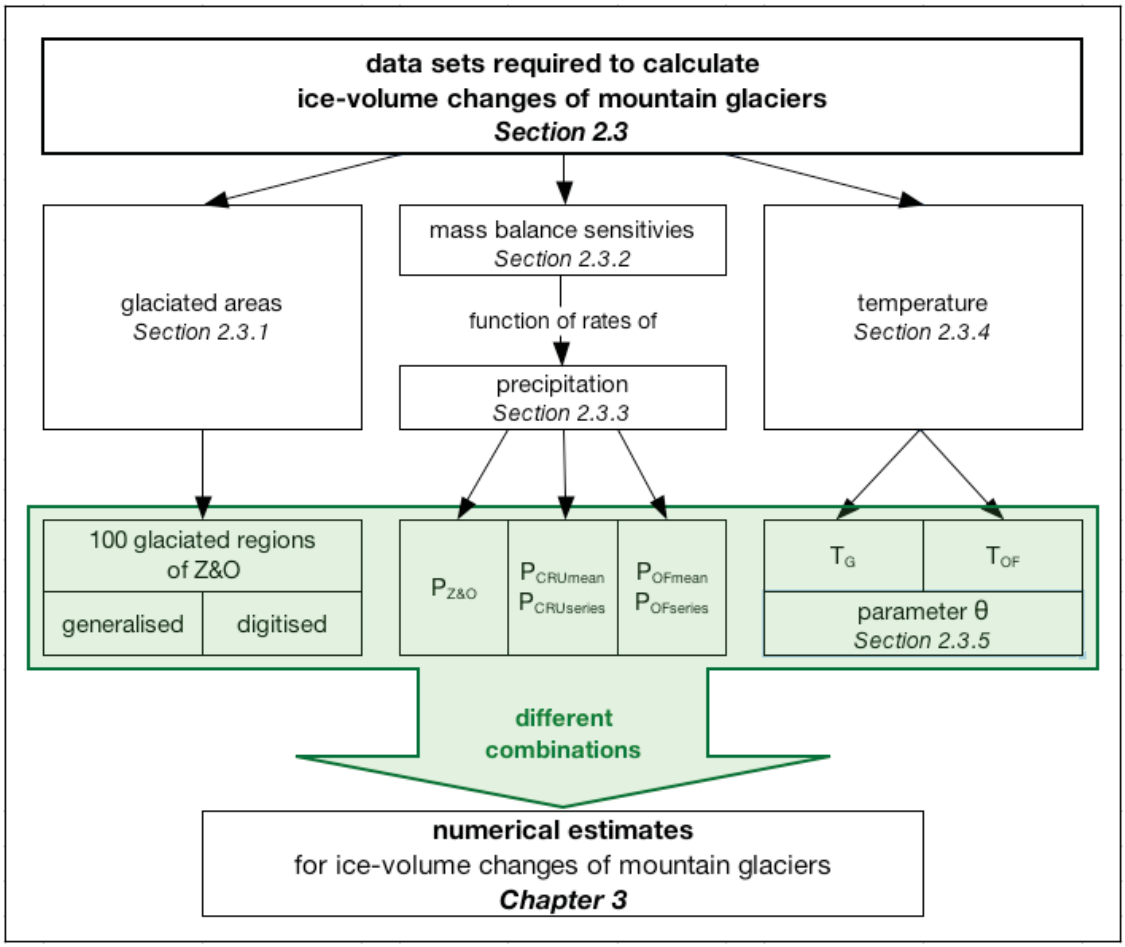

Figure 2.5: Flowchart showing the available data sets (discussed in more detail in the text) used to numerically estimate ice-volume changes of mountain glaciers. The locations and areas of 100 glaciated regions are taken from Zuo and Oerlemans (1997a) (Z&O), however a distinction of this *generalised* data set to a *digitised* area representation (in Alaska and Svalbard) is made. Precipitation data sets of Zuo and Oerlemans (1997a) ($P_{Z\&O}$), the Climate Research Unit ($P_{CRUaver}$ and $P_{CRUseries}$), and from Siobhan O'Farrell (P_{OFaver} and $P_{OFseries}$) are available for the determination of mass balance sensitivities. Two temperature data sets provided by Jonathan Gregory (T_G) and Siobhan O'Farrell (T_{OF}) are available. In connection with temperature, the imbalance between climate and glacier state Θ is discussed and constrained. Several combinations of these data sets and parameter settings (green area) lead to a range of estimates for ice-volume changes of mountain glaciers (*numerical estimates*) discussed in Chapter 3.

2.3 Global data sets

Having established the numerical model of mountain deglaciation in the previous section (Equation 2.3), we now need reliable data as input to the model. In this section a variety of data sources is evaluated and where possible compared to observational data. Several different data sets have been selected to drive the model and Figure 2.5 illustrates the overall approach of combining data sets for estimating ice-volume changes (outcomes are also denoted "deglaciation models" in this thesis).

2.3.1 Area of glaciated regions

According to Church et al. (2001) there are more than 160,000 glaciers and 70 ice caps world wide. These glaciers can be climatically grouped to 100 glaciated regions (as in Oerlemans, 1993; Zuo and Oerlemans, 1997a, updated the data set). The areas and approximate locations of the 100 glaciated regions are listed in Table A.1 on pages 301-304. The total area is estimated to be 527,728 km^2. The data is 'based on Haeberli et al. (1989), with additions, and on climatological maps, tables and compilations of various kinds' (Oerlemans, 1993, p. 115). It does not include any independent glaciers at the periphery of the Greenland and Antarctic ice sheets. As shown in Figure 2.6, the area of glaciers around the two major ice sheets make up about 30% of the total. A discussion on these glaciers is given separately but since the required information on the glaciers in these regions is not available to me, results from other studies are presented only.

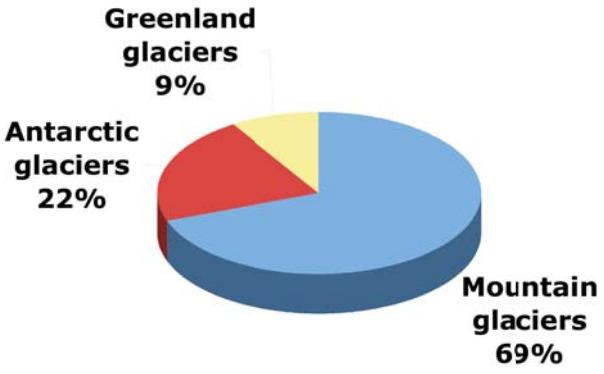

Figure 2.6: Area distribution of mountain glaciers and peripheral glaciers of the Antarctic and Greenland ice sheets (data taken from Dyurgerov and Meier, 2005).

Oerlemans (1993) noted that this data set of 100 glaciated regions might not be accurate in all its detail, but can be used for basic global estimates. Detailed information of the shape of each of the 100 glaciated regions is not available. Therefore, a square with the area given in Zuo and Oerlemans (1997a) is centred

over the listed location and is used as a spatial representation (illustrated with red squares in Figure 2.7). This spatial distribution of glaciated areas is denoted *generalised data set* in this thesis.

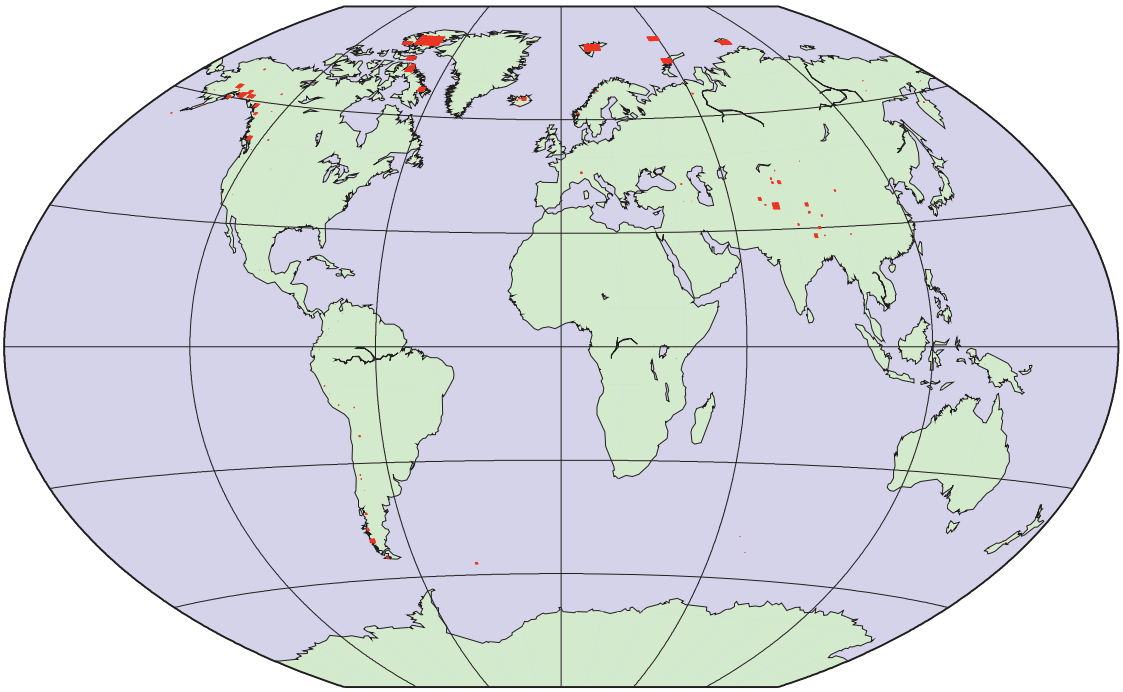

Figure 2.7: Red boxes represent the locations and extents of 100 glaciated regions of the so-called generalised data set taken over from Zuo and Oerlemans (1997a).

Both the volume and area of a glacier respond to climatic change. Chen and Ohmura (1990) developed an empirical formula relating the volume V (in km^3) of alpine glaciers to their surface area S (in km^2) of $V = 0.0285 \times S^{1.357}$ and concluded that the volume of alpine glaciers decreased by 29% from the 1870s to the 1970s (with an area loss of 33%). They also derived a relationship between changes in volume ΔV of a mountain glacier to changes in the surface area ΔS by calculating the derivative of the above equation: $\Delta V = 0.038716 \times S^{0.357} \Delta S$. Bahr et al. (1997) obtained a similar relationship between volume and surface area of glaciers, with a slightly different power: $V \propto S^{1.375}$. For ice caps and ice sheets, the relationship $V \propto S^{1.25}$ was found. However, Bahr et al. (1997) did not present the proportionality factors. The recent study by Radić et al. (2007) derived a relationship of $log\, V = 1.56\, log\, A - 2.11$ based on analyses of 37 synthetic glaciers of different sizes. Meier (1984) estimated the areal shrinkage of glaciers in 13 regions to be 5 to 44% in 61 years based on observed long-term changes. However, note that in areas of larger ice cover (e.g. Canada and Alaska) the shrinkage has been less than in those areas where most of the observations have been made (e.g. Alps and Scandinavia), and therefore the estimate for the global areal shrinkage may be

different. Van de Wal and Wild (2001) found that when assuming a constant glacier area over time in the mass balance calculation, an overestimation of the volume change by around 20% is the consequence. However, Van de Wal and Wild (2001) also noted that only 41 glaciated regions (covering 38% of the total area) have available size distributions[8], and this consequently limits the robustness of global estimates. In the case study of the Hintereisferner (Austria) by Raper et al. (2000) the relative change in area between the mean values over the periods 1892-1921 and 1961-1990 is 25% at maximum.

In general, the relationship between changes in a glacier's area and volume will not be considered here. Hence, the glacier area in all further analyses will be held constant over time. This weakness in the model is unavoidable at present as the required detailed information (i.e. area and/or volume of individual glaciers) is not available within all glaciated regions. However, an evaluation of the potential effect of this simplification on future projections for a few glaciated regions will be presented in Chapter 8.

The generalisation in areal representation of glaciers (a square) will result in inaccuracies in the predictions of geodetic signals because of their sensitivity to the distribution of the changing ice load and the distance to the observing site (as will be shown in Section 5.2). Therefore, glaciers in Alaska and bordering Canada (Section 2.3.1.1) and on the Svalbard archipelago (Section 2.3.1.2) have been digitised in order to investigate the impact on geodetic signals, in particular in the near-field, of using the detailed (denoted *digitised data set* in the following) or the generalised area-representation of glaciated regions (in Section 5.2). It is likely that this high resolution distribution of glaciers will lead to improved predictions of geodetic signals in these areas.

2.3.1.1 Glaciated regions in Alaska and bordering Canada

According to the U.S. Geological Survey[9], there are ∼100,000 glaciers in the State of Alaska, covering about 5% of the landscape (Molnia, 2007). In the data set of Zuo and Oerlemans (1997a) they represent about 17% of the total area of mountain glaciers world wide. The area of Alaska's glacier systems and glaciers along the Canadian border have been digitised with a resolution of 0.1° from the Times Atlas published in 1988 at a scale of 1:5,000,000 (Times Atlas, 1988, page 113).

[8] A size distribution of a glaciated region is defined by the number of glaciers in a size class and the mean area. The sizes of the classes are: 2^{-6}–2^{-5} km^2, 2^{-5}–2^{-4} km^2, ..., $\geq 2^9$ km^2.

[9] http://www.usgs.gov/faq/list_faq_by_category/get_answer.asp?id=296

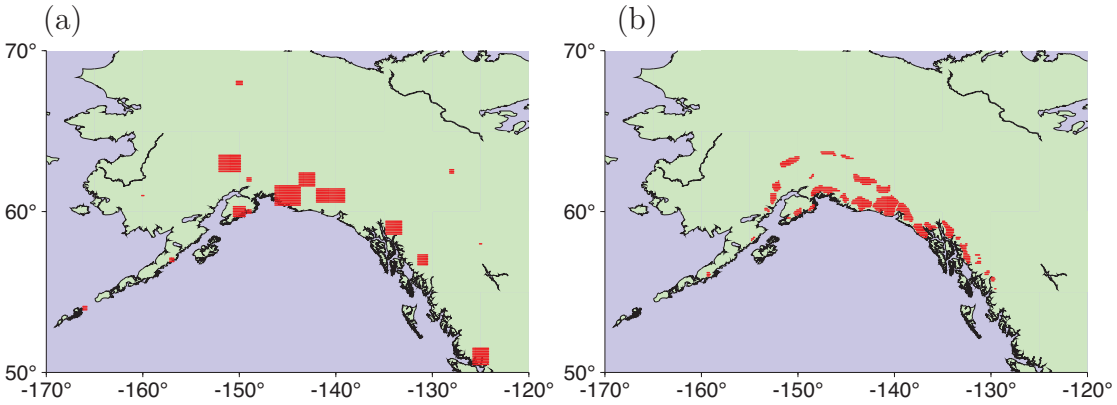

Figure 2.8: Comparison of locations and spatial distribution of glaciated regions in Alaska and bordering Canada between (a) the generalised data set as defined by Zuo and Oerlemans (1997a) and (b) the digitised data set. A topographic representation is given in Figure B.1 on page 306.

Figure 2.8 shows the differences in size and location of glaciated regions in Alaska and Canada between the generalised and the digitised data set. Whereas the glacier area of the generalised data set in Alaska and bordering Canada is 90,732 km^2 (Zuo and Oerlemans, 1997a), the area of the digitised glaciers is only 79,353 km^2. This is a reduction of more than 12%. As the publication date of the two sources is almost the same, one reason for the difference in glacier area may lie in the under-representation of glaciated areas in the map used for the digitisation. Another study of Alaska's glaciers by Molnia (2007), in turn, state a glacial area of about 75,000 km^2 based on sources from the 1970s and early 1980s. Overall, the area determined by Zuo and Oerlemans (1997a) is expected to be more representative of the true glacier-cover in Alaska, since it is based on the detailed information of the World Glacier Inventory (Haeberli et al., 1989) rather than on a larger-scale map reconstruction as in the case of the Times Atlas (1988).

2.3.1.2 Glaciated regions in Svalbard

The archipelago of Svalbard is another region where glaciers cover large areas of land (about 60% of the islands). Svalbard's glaciers comprise almost 7% of the total area of mountain glaciers world wide. As in the case of Alaska, the boundaries of the ice fields of Svalbard have been digitised at a 0.1° resolution in order to get a more accurate representation of the glacier distribution (see Figure 2.9). The map used for the digitisation, at a scale of 1:1,000,000, was published in 1986 by the Department of Geography in Oslo. Here, the difference in area between the two data sets is smaller. According to Zuo and Oerlemans (1997a) Svalbard's glaciated

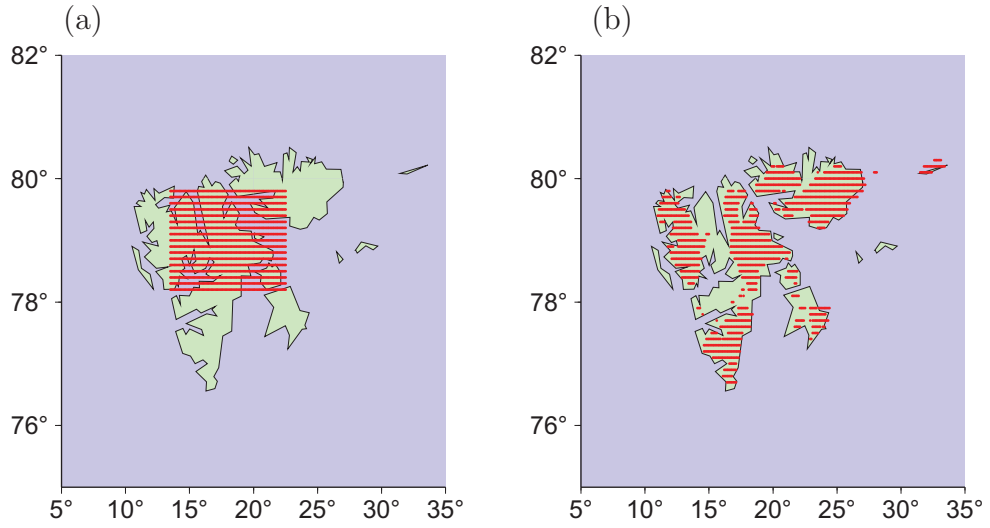

Figure 2.9: Comparison of locations and spatial distribution of glaciated regions of the Svalbard archipelago between (a) the generalised data set as defined by Zuo and Oerlemans (1997a) and (b) the digitised data set. A topographic representation is given in Figure B.2 on page 307.

area is 36,600 km^2 and is represented as one single square in the generalised data set (Figure 2.9a). In the digitised data set the glaciers in Svalbard have an area of 35,700 km^2.

2.3.1.3 Glaciers at the periphery of the Antarctic and Greenland ice sheets

Numerous, seemingly independent local glaciers surround the Antarctic and Greenland ice sheets. Weidick and Morris (1998) apply the term *local glaciers* to all types of ice cover across Greenland and Antarctica, i.e. to glaciers in the form of ice caps, valley glaciers, mountain glaciers etc., with the exception of the continental ice sheet (the *Inland ice*). These local glaciers not only occur on the coastal "ice-free" areas, but also on the nunataks of the Inland ice. Weidick and Morris (1998) classify these local glaciers into three categories:

(i) glaciers that are situated on the *"ice-free" coast* or on *offshore islands*. These behave essentially in the same way as most other glaciers around the world.

(ii) *fringing* ice caps or ice fields which are defined by the location of ice divides and by the surrounding and subglacial topography. Their mergence to the ice sheet is so extreme that inland parts of these glaciers largely contribute to the nearby ice sheet outlets, whereas coastal parts must more or less be regarded as local glaciers.

(iii) *ice domes* or glaciers within the ice-marginal zone and on the *nunataks* of the ice sheet. These glaciers are intimately linked to the ice sheet and their response could not be regarded as local and hence these glaciers can be seen as part of the Inland ice.

Weidick and Morris (1998) consider only the first category as "true" local glaciers. They argue the necessity for future work to establish mass-balance estimates of these glaciers. In particular for Antarctica, the primary need is mapping on a sufficiently detailed scale to resolve the form of local glaciers to enable more precise estimates of their area. Weidick and Morris (1998) concluded on the basis of other studies that the area of local glaciers associated with each of the two ice sheets is comparable and around 70,000 km^2. However, later analyses (e.g. Dyurgerov and Meier, 2005) suggest that the total area of the independent local glaciers around the Antarctic ice sheet may be much greater, $\sim$169,000 km^2, or more than double that of the Greenland ice sheet.

2.3.2 Mass balance sensitivity

In order to calculate ice-volume changes of mountain glaciers using Equation 2.3, the sensitivities of glacier mass balance rates to temperature changes are required. The change in mass balance due to temperature changes is dependent on the elevation (small mass balance change in accumulation area and largest in the ablation area). Dynamic sensitivity analyses require knowledge of the changing glacier geometry with time (Oerlemans et al., 1998) and at present this data is mostly unavailable. Hence, only the *static temperature sensitivity* (Braithwaite and Zhang, 1999a) is considered here, which is an average over the glacier area. Static sensitivity can be used to make first estimates of changes in glacier volume to given climate scenarios. Sensitivity studies of glacier mass balance determined by energy-balance modelling have been, amongst others, undertaken by Oerlemans and Fortuin (1992), Zuo and Oerlemans (1997a), and Oerlemans (2001) and these are discussed in the following paragraphs.

Sensitivity experiments undertaken by Oerlemans and Fortuin (1992) of 12 glaciers (listed in Table 2.1) for which detailed mass balance observations exist show changes in mean specific mass balance rates of between -0.12 and -1.15 m year^{-1} (red diamonds in Figure 2.10) for an increase in temperature throughout the year of 1 K. These 12 glaciers are only a small part of all glaciers for which mass balance measurements have been performed. However, Oerlemans and Fortuin (1992) argue

that they represent a wide range of climatological settings in which glaciers and small ice caps are found, with the exception of the tropics.

According to Oerlemans and Fortuin (1992), the only significant relation between these mass balance sensitivities and climatic or geographical parameters can be found with annual precipitation. Therefore, in Figure 2.10 the effect of a 1 K warming on the mean specific mass balance rates of the 12 selected glaciers is plotted against annual precipitation. Subsequently, Oerlemans and Fortuin (1992) fitted the data points with the following logarithmic curve (red solid curve in Figure 2.10):

$$\Psi(\Delta T) = -0.512 - 0.662 \times log(p) \tag{2.4}$$

where p is the annual average precipitation over the glacier in meters year^{-1}. This result is in close conformance with the study by Braithwaite et al. (2002), which is based on mass balance sensitivities for 61 glaciers calculated by a degree-day model. According to Oerlemans and Fortuin (1992) Equation 2.4 is only valid for:

$$p \geq 0.22\ m\ \ year^{-1} \tag{2.5}$$

They assert that glaciers in general form in the wettest part of a terrain where pronounced topography results in higher precipitation rates than the local average. Therefore, precipitation rates taken from maps and weather stations (labelled P in Equation 2.6) may underestimate the precipitation at the actual glacier. Oerlemans and Fortuin (1992) recommended to adjust these precipitation rates by adding 25%, i.e. introducing an effective annual average precipitation of

$$p = P \times 1.25 \tag{2.6}$$

It is difficult to assess the correctness of this assumption and hence Oerlemans (2001, p. 115) note that 'the correction applied, +25%, is just a guess, however'.

The approximation of mass balance sensitivities in Equation 2.4 with the condition of Equation 2.5 and 2.6, allows the determination of sensitivity estimates for other glaciers, provided that precipitation data is available. However, it needs to be noted here that the fitted curve is still based on results from only 12 glaciers and the validity of upscaling to a global scale relies on the assumption that the mass balance sensitivity is determined solely by precipitation (Braithwaite and Zhang, 1999a; Braithwaite et al., 2002). Furthermore, it is questionable if a logarithmic fit

glacier	area	ela	prec	
Abramov central Asia	25.9	4212	0.96	valley glacier
Tuyuksu central Asia	3.1	3888	1.30	valley glacier
Peyto Canada	12	2682	1.85	valley glacier
Devon ice cap Canadian Arctic	1695.1	1137	0.22	4% tidewater glacier
White glacier Canadian Arctic	38.9	1006	0.30	valley glacier
Engabreen northern Norway	32.0	1003	5.30	outlet glacier of Svartisen ice cap
Nigardsbreen southern Norway	48.2	1534	4.19	valley glacier, outlet of Jostedalsbreen
Hellstugubreen southern Norway	3.1	1912	2.49	valley glacier, outlet of Jotunheimen
Alfotbreen southern Norway	4.8	1186	7.00	valley glacier
Rhone glacier Switzerland	18.5	2854	2.68	valley glacier
Gries glacier Switzerland	6.3	2883	1.75	valley glacier
Hintereisferner Austria	9.7	2972	1.91	valley glacier

Table 2.1: List of glaciers studied by Oerlemans and Fortuin (1992), Zuo and Oerlemans (1997a), and Oerlemans (2001) to develop a relationship between mass balance sensitivities and annual precipitation. The area is given in km^2, the equilibrium-line altitude (ela) in meter, and the annual precipitation (prec) is given in meter $year^{-1}$.

is physically sensible in order to approximate the glacier's mass balance sensitivity (see the curve fit of Oerlemans and Fortuin (1992) in Figure 2.10), in particular as extrapolation outside the data region can become unrealistic.

A second study of the same 12 observed glacier mass balances was undertaken by Zuo and Oerlemans (1997a). Here, the relation between mass balance sensitivity and annual precipitation was approximated by

$$\Psi(\Delta T) = \alpha \, p^{\beta} \tag{2.7}$$

where α and β are constants fitting the 12 observed glaciers. Zuo and Oerlemans (1997a) determined values for α and β and furthermore, made a distinction between summer and non-summer mass balances sensitivities. The annual mass balance

sensitivity was found to be

$$\Psi(\Delta T_a) = -0.387\, p^{0.683} \tag{2.8}$$

Zuo and Oerlemans (1997a) analysed the effect on mass balance when changing only the summer temperature and consequently found

$$\Psi(\Delta T_s) = -0.259\, p^{0.427} \tag{2.9}$$

The mass balance sensitivity to non-summer temperature variations is approximated by the difference between the sensitivities to annual and to summer temperature changes, i.e.

$$\Psi(\Delta T_{ns}) = \Psi(\Delta T_a) - \Psi(\Delta T_s) \tag{2.10}$$

The corresponding curves are plotted against annual precipitation in Figure 2.10 (in blue). The dashed curves in the figure represent the summer and non-summer mass balance sensitivities. The curves show that glaciers with relatively small precipitation rates are predicted to be more sensitive to changes in summer temperature than to non-summer temperature variations. In contrast, glaciers with at least 3 m year^{-1} precipitation are more sensitive to changes in non-summer temperature.

Oerlemans (2001) modified (without details) the above mass balance model and added a 13^{th} glacier (Storglaciären, Sweden) to the analysis. The resulting mass balance sensitivities for the 13 glaciers are plotted against annual precipitation in Figure 2.10 (green dots). Significant differences to the previous studies can be observed, which also has an effect on the resulting power law fit for annual mass balance sensitivity. In Oerlemans (2001) this is defined as

$$\Psi(\Delta T_a) = -0.271\, p^{0.597} \tag{2.11}$$

and is plotted in green in Figure 2.10.

Observations on glaciers show that those located in wetter regimes (e.g. glaciers in New Zealand and maritime parts of Alaska) are most sensitive to climatic changes. This is also represented in the various approximations of Oerlemans and Fortuin (1992), Zuo and Oerlemans (1997a), and Oerlemans (2001). Glaciers in regions of high precipitation have a higher mass turnover and extend to lower altitudes, where the temperature is above freezing for most of the year. Consequently they

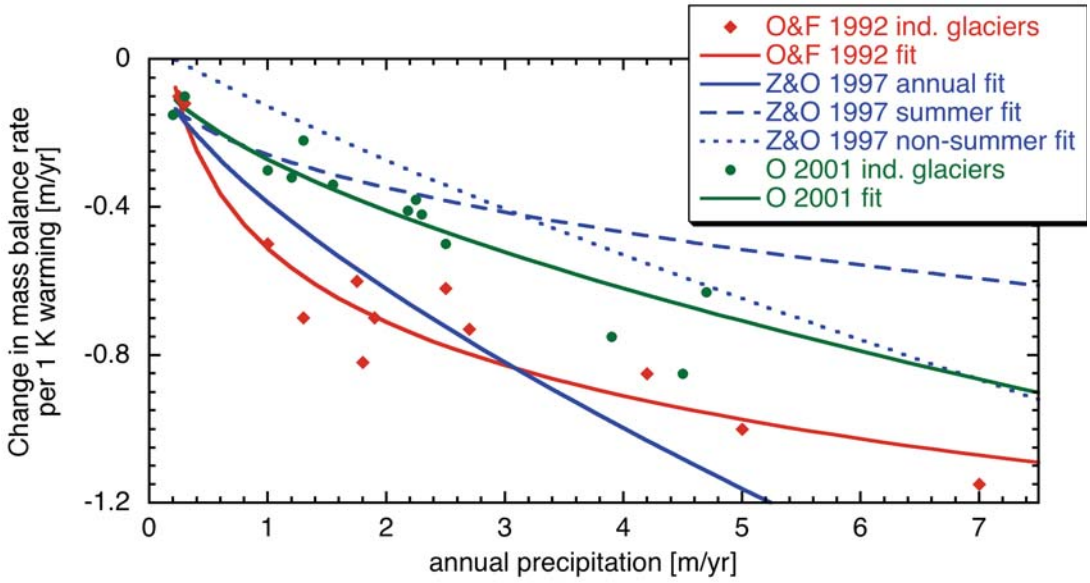

Figure 2.10: Mass balance sensitivities of 12 glaciers per 1 K warming as a function of annual precipitation as defined by Oerlemans and Fortuin (1992) represented by red diamonds. Fitted curves through the 12 data points of Oerlemans and Fortuin (1992) and Zuo and Oerlemans (1997a) are represented in solid red and solid blue, respectively. Additionally, Zuo and Oerlemans (1997a) developed mass balance sensitivities to summer and non-summer temperatures (dashed curves). Oerlemans (2001) modified the mass balance model (green dots), added a 13^{th} glacier, and fitted another curve to the data points (solid green curve).

have a greater sensitivity to temperature changes. In order words, variations in mass balance sensitivities reflect differences in mean precipitation between different regions (Braithwaite and Zhang, 1999b). The increased sensitivity to temperature variations of glaciers in wetter environments is mainly due to three factors (Oerlemans, 2001):

- ➢ a stronger albedo feedback
- ➢ larger effect on the partitioning of precipitation between snow and rain
- ➢ longer ablation seasons as glaciers extent down to lower altitudes

To summarise, temperature and precipitation play important roles in estimating mass balances of mountain glaciers, especially when no direct observations are available. The established numerical relationships between mass balance sensitivities to temperature changes and annual precipitation can be used to determine the mass balance sensitivities of glaciers where only precipitation data is available. However, Oerlemans (2001) states that this relation should be used with caution as for individual glaciers it may only provide first-order estimates. For all further calculations, the models of mass balance sensitivities to changes in summer and non-summer temperatures as determined by Zuo and Oerlemans (1997a) will

be used (Equation 2.9 and 2.10). Thus, a seasonally differentiated approach in the calculation of ice-volume changes is introduced.

2.3.3 Precipitation data

Glacier-climate modelling indicate that temperature changes have a generally greater impact on variations in glacier mass than precipitation changes. However, there are local exceptions to the general rule. For example, precipitation changes on ice masses in maritime environments have a greater variability, in particular on interannual time scales, compared to temperature variations (Marshall, 2006). Therefore, precipitation variability can also have a significant effect on mass balance fluctuations. Furthermore, as established in the previous section, the amount of precipitation on a glacier appears to determine the sensitivity of the mass balance to climate changes and hence is required for the calculation of ice-volume changes in Equation 2.3.

Two different approaches for obtaining annual precipitation rates in glaciated regions based on three different sources of data are established. These sources are:

1. **Zuo and Oerlemans (1997a)**. This data set provides annual precipitation rates for 100 glaciated regions; the numbers are listed in Table B.2 on page 311 (labelled as $Z\&O$) and also in Table A.1 on pages 301-304. This compilation is based on Climatic Atlases (1970) of Europe, North America, Asia etc. and are valid for the period before 1970.

2. Climate Research Unit, **CRU**. This data set is based on historical monthly precipitation for global land areas from 1900 to 1998. A total of 1520 land gridboxes is derived at a 2.5° latitude by 3.75° longitude resolution from some 12,000 land gauge records (Hulme et al., 1998). A detailed description of the gridding method is available on the CRU web page[10]. This data set includes nearly 30 years more data than given by Zuo and Oerlemans (1997a). However, the observation intervals of the available time series of the CRU data set vary greatly.

3. Siobhan **O'Farrell**[11]. This modelled data set is developed at the CSIRO Marine and Atmospheric Research Centre[12] using the Mk3.5 climate system

[10] http://www.cru.uea.ac.uk/
[11] http://www.dar.csiro.au/profile/ofarrell.html
[12] http://www.cmar.csiro.au/

model (the Mk3.5 model is an improved version of the Mk3 model; Gordon et al., 2002). The scheme of precipitation includes the processes of autoconversion[13] and collection of cloud liquid water by falling rain and snow described in detail in Rotstayn (1997). The data is given on a monthly basis from 1871 onwards and hence provides at least 30 more years of data compared to the previous two sources. The longitude spacing is 1.875 degrees, latitude spacing is ∼1.86 degrees, and the data is given in mm per day.

The last two data sets are given in form of time series and therefore two approaches for developing annual precipitation rates are determined for each. The first consists of *average annual means* for a particular time period which ignores the change in precipitation with time during the interval. Mass balance models need to consider changes in not only temperature but also precipitation, as the climatic controls of glacier mass balance differ in all regions and the patterns and rates of predicted climate change also differ significantly between regions. Therefore, the second approach is based on developing *time series* of annual precipitation rates. The standard deviation σ of any trend calculated from these time series is derived from

$$\sigma^2 = \frac{\Sigma \Delta y_i^2}{n-2} \, \frac{n}{n\,\Sigma t_i^2 - (\Sigma t_i)^2} \tag{2.12}$$

assuming that all n data points are statistically independent[14]. $\Sigma\Delta y_i$ are the residuals of the trend line at times t_i and n is the total number of years with available precipitation data.

The five different data sets of precipitation rates are briefly explained and analysed for comparison in the following.

1. **Annual precipitation by Zuo and Oerlemans (1997a)**
   The first approach in obtaining a precipitation data set for 100 glaciated regions uses the values derived by Zuo and Oerlemans (1997a) and is labelled $\mathbf{P}_{\boldsymbol{Z\&O}}$ in this thesis. These data are based on observations made before 1970 and are not necessarily representative after that time, although Zuo and Oerlemans (1997a) use this precipitation data set for their calculations over the period from 1865 to 1990.

[13] autoconversion refers to the growth of cloud droplets into precipitation drops by collision and coalescence

[14] This assumption may result in an underestimation of the standard deviation (Emery and Thomson, 1997).

2. **Average annual mean precipitation of the CRU data set**
   The second way of determining annual precipitation rates is based on the observed precipitation data set from the CRU. With the time series of monthly precipitation, average annual mean precipitation has been calculated for each grid point (Figure 2.11). Only years with available data for all 12 months have been used. This data set is denoted by $\mathbf{P}_{CRUaver}$ in this thesis.

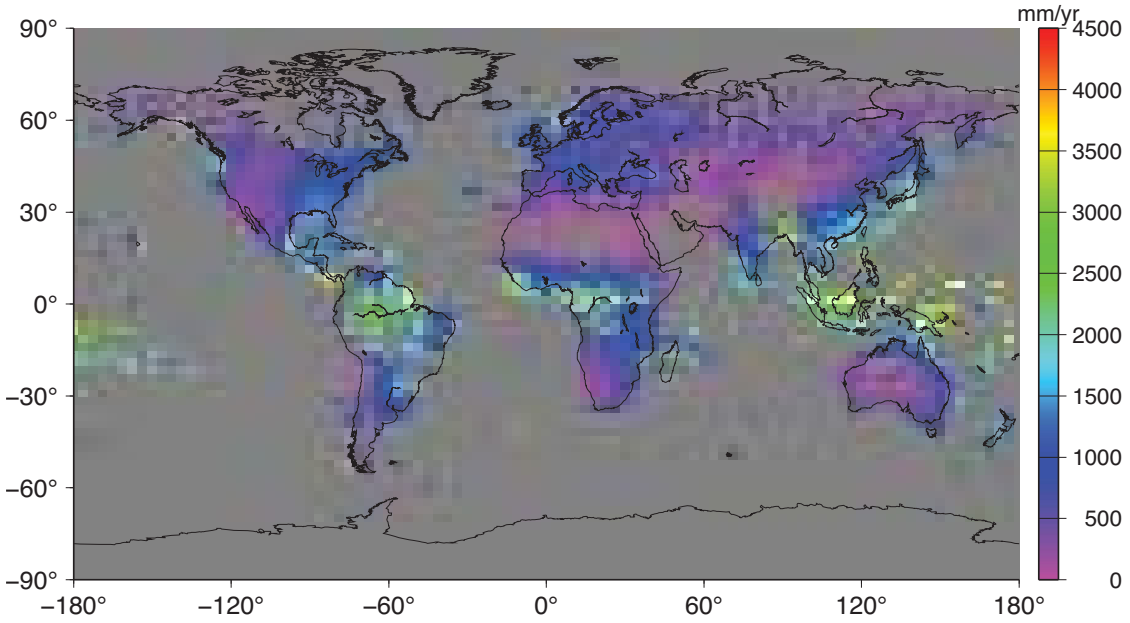

Figure 2.11: Average annual mean precipitation in mm year^{-1} over the period 1900-1998 (or for the period with available data). The data is taken from the Climate Research Unit (CRU) and is based on historical monthly precipitation observations.

The average annual mean precipitation for the 100 glaciated regions were calculated using precipitation data from the grid in closest proximity to each region. The resulting values for the 100 glaciated regions are derived for different time periods because the data distribution is not identical for all regions. For the 100 glaciated regions, available data periods range between 24 and 97 years with a mean of 84 years. Despite this variability, the derived means are assumed to be representative for any required period in the following.

The approximate distances between the centres of the glaciated regions and the locations of available precipitation data are listed in the last column in Table B.1 on page 309. For two glaciated regions (#52 South Atlantic Islands and #60 Novaya Zemlya) the closest grids with available precipitation data are at distances of ∼670 and ∼760 km, respectively. For a further 12 glaciated regions the closest gridboxes with available precipitation data are at distances

between 300 and 440 km. The remaining regions have precipitation data at grid cells within a distance of less than 300 km to the glaciated area.

Table B.2 on page 311 lists average annual mean precipitation rates of 100 glaciated regions derived from the CRU data set described above. Precipitation rates have been corrected according to Equation 2.6 by adding 25% to account for the under-representation of precipitation rates at weather stations. Furthermore, CRU precipitation rates less than 0.22 m year^{-1} have been set to that value (see Equation 2.5). This limit has to be taken into account in the analyses of mass balance sensitivities because the logarithmic fit (Equations 2.9 and 2.10) determined by Zuo and Oerlemans (1997a) is only valid for annual precipitation greater than 0.22 m year^{-1}.

3. **Time series of observed CRU precipitation**
   With the available precipitation time series of the CRU, a second approach is developed here using actual time series of precipitation rates for each region (this data set is labelled $\mathbf{P}_{\boldsymbol{CRUseries}}$) instead of a single average annual mean. This is considered necessary as several of the 100 glaciated regions have linear trends in annual precipitation over time (although not always statistically significant at a 2σ level, see Table B.3 on page 313), which may have a significant effect on any subsequent calculations. For example, precipitation in the northern Cordillera (#40), where data for 46 years are available, show a trend of approximately $+20\pm8$ mm year^{-2}. In this case, the nearest gridbox of precipitation data linked to that glaciated region is located more than 200 km away from the centre of the glaciated region. The South Atlantic Islands (#52) also show a relatively large positive trend in the precipitation. However, the gridbox for the corresponding precipitation data is almost 700 km away. The time series of precipitation data at the Chugach Mountains (#16) in Alaska show a high negative trend of -12 ± 3 mm year^{-2} with available data over 97 years. These results suggest that time series rather than long-term averages of precipitation data should be used in further calculations.

4. **Average annual mean precipitation of the O'Farrell data set**
   Figure 2.12 shows the calculated average annual means of the O'Farrell precipitation data set for the period from 1871 to 2000. Here, similar spatial patterns to the CRU data set (Figure 2.11) can be seen. The advantage of the O'Farrell data set is that it is spatially and temporally complete.

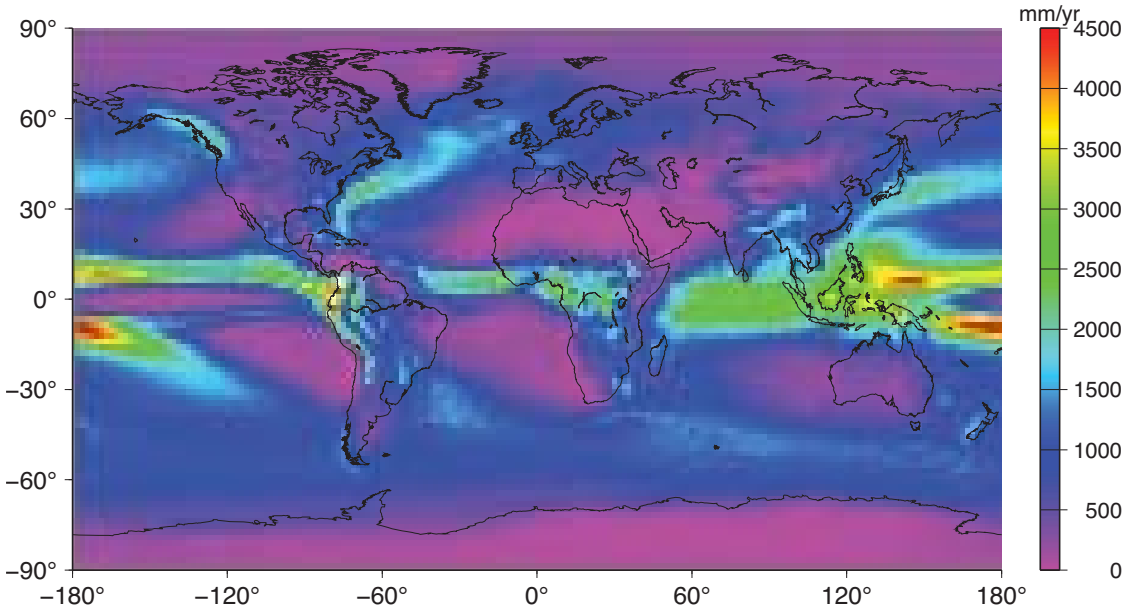

Figure 2.12: Average annual mean precipitation in mm year^{-1} over the period 1871-2000 provided by O'Farrell.

Average annual means for the 100 glaciated regions have been calculated from this data set (labelled $\mathbf{P}_{OFaver}$ in the following) and are compared to those of Zuo and Oerlemans (1997a) and of the CRU data set in Table B.2 on page 311. The correction factor of Equation 2.6 is applied here as well as the adjustment of those precipitation rates smaller than 0.22 m year^{-1} (Equation 2.5).

5. **Time series of modelled precipitation by O'Farrell**
   With the modelled data set of precipitation rates of O'Farrell for the period 1871-2000, time series of annual means have been determined (labelled $\mathbf{P}_{OFseries}$ in this thesis). Linear trends for these time series over the period 1871-2000 are listed for the 100 glaciated regions in Table B.4 on page 314 and show small variations in magnitude between regions. However, in approximately half of the regions, the trend is statistically significant (on a 1σ level) different from zero. Hence, a possible effect on any following calculations is feasible. The calculated linear trend at the Coast Mountains (#18) in Alaska/Canada is $+1.9\pm0.6$ mm year^{-2} and represents the maximum value within the 100 glaciated regions.

Comparison of precipitation data sets

Comparing $P_{Z\&O}$ and $P_{CRUaver}$ in Table B.2 show that for only 19 of the 100 glaciated regions do the values agree within 25%. 79 of the 100 glaciated regions have $P_{CRUaver}$ values that are lower than those of $P_{Z\&O}$. Assessing the P_{OFaver} rates show that 30 glaciated regions fit within 25% to the estimates of $P_{Z\&O}$. In 47 of the regions, the values of P_{OFaver} are higher than those of $P_{Z\&O}$. The histograms in Figure 2.13 compare the average annual mean precipitation of $P_{Z\&O}$, $P_{CRUaver}$, and P_{OFaver} and demonstrate the degree of variability in estimates. Precipitation rates vary according to whether they are primarily based on observational data or on numerical models. Another reason for different estimates of average annual mean precipitation in a region is that the three data sets cover different time spans (see beginning of this section).

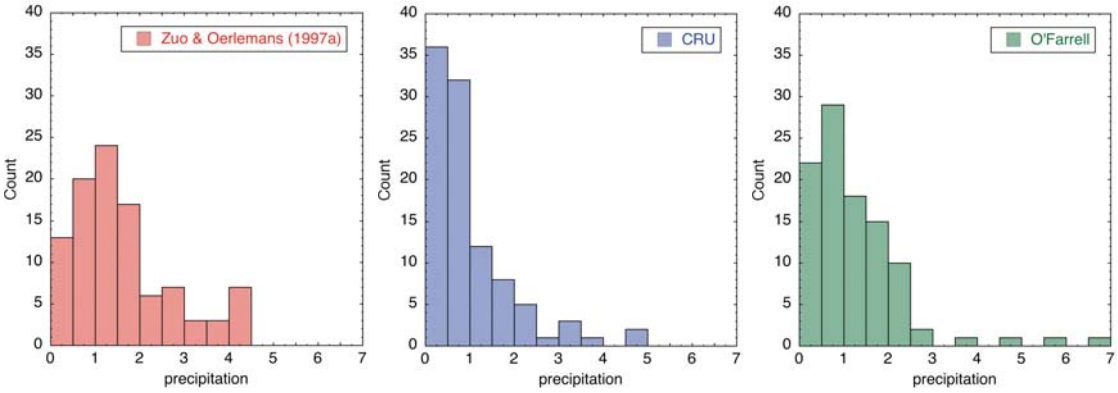

Figure 2.13: Histograms of average annual mean precipitation in meters year^{-1} of water for 100 glaciated regions of Zuo and Oerlemans (1997a), calculated from the Climate Research Unit (CRU) data set and from the data set of O'Farrell.

The numbers in Table B.2 do not clearly indicate which data set best represents the precipitation in glaciated regions. The average annual precipitation in Zuo and Oerlemans (1997a) of 100 glaciated regions is 1.49 m year^{-1}. Using the CRU precipitation data set under consideration of Equation 2.5 and 2.6, the total average annual precipitation for the same 100 glaciated regions is only 1.00 m year^{-1} . The total average of the O'Farrell data set is 1.28 m year^{-1}. Overall, the O'Farrell data set (based on a numerical model) matches the observational data set of Zuo and Oerlemans (1997a) better than the CRU data set (as is also reflected in the histograms of Figure 2.13). Furthermore, although the CRU data set is based on observations, the O'Farrell data set has the advantage that it is spatially and temporally complete. Nevertheless, for further analyses purposes, all five data sets of precipitation rates are used in the following chapter.

2.3.4 Temperature data

The effect of a temperature increase on a glacier is an expansion of the ablation area, a lengthening of the melt season, an increase of the extent of melt at a given site, and an increase of the proportion of precipitation that falls as rain rather than snow. In order to quantitatively calculate ice-volume changes of mountain glaciers using Equation 2.3, time series of temperature variations are required. Two modelled temperature data sets, provided by Jonathan Gregory and Siobhan O'Farrell, are used in this study and are labelled $\mathbf{T_G}$ and $\mathbf{T_{OF}}$, respectively.

The temperature data set provided by **Jonathan Gregory**[15] is based on the Hadley Centre model of the climate system (Stott et al., 2000)[16]. This model (HadCM3) consists of an Atmosphere General Circulation Model (AGCM), coupled to an Ocean General Circulation Model (OGCM)[17]. It includes both the most important anthropogenic forcings and natural forcings during the 20^{th} century. The simulations include parameters used to estimate the level of greenhouse gases, including carbon dioxide and methane, tropospheric and stratospheric ozone, and sulfur emissions. Natural forcings due to changes in the amount of stratospheric aerosols following explosive volcanic eruptions and spectrally resolved changes in solar irradiance are also included. The HadCM3 model assumes that future emissions of greenhouse gases will follow the IS92a scenario (IPCC, 2001), in which the atmospheric concentration of carbon dioxide more than doubles over the course of the 21^{st} century. The model assumes mid-range economic growth but no measures to reduce greenhouse-gas emissions. Although this model runs into the future, only temperature data for the past were made available to this study. This data contains monthly surface air temperatures in Kelvin for the period December 1859 until November 1997. Grid spacing is 3.75 degrees in longitude and 2.5 degrees in latitude.

The HadCM3 data set presents one result of a particular climate modelling scenario. **Siobhan O'Farrell** provided another data set of modelled temperature developed from a transient run with changing greenhouse gases and aerosols using the CSIRO Mk3.5 climate system model (Gordon et al., 2002, see also Section 2.3.3 on page 40). Different atmospheric and ocean models and different physical packages and parameter settings for the 20^{th} and 21^{st} century are used for this run, resulting

[15] University of Reading and Hadley Centre, UK, http://www.met.rdg.ac.uk/∼jonathan

[16] reference also at http://www.metoffice.com/research/hadleycentre/

[17] Atmosphere-Ocean General Circulation Model: numerical representation of the climate system based on the physical, chemical, and biological properties of its components, their interactions and feedback processes, and accounting for all or some of its known properties.

in an independent climate model to the one of the Hadley Centre. Differences in the two models also include solar and volcanic forcing as well as climate sensitivities (Gordon et al., 2002). In this data set, projected monthly temperature is given for the period 1871 until 2100. Grid spacing in longitudinal direction is 1.875 degrees and the latitude spacing is ∼1.86 degrees.

2.3.4.1 Large scale temperature variations

To gain further insights from the two global models of temperature variations with time, the Earth has been divided into 8 sectors and mean annual temperature series for each sector have been calculated. The longitudinal division of the sectors is listed in Table 2.2. During the averaging process the temperature data have been weighted by grid cell area.

Figure 2.14 illustrates time series of mean annual temperature of the Gregory and O'Farrell data sets for the various sectors with the northern and the southern hemispheres in separate panels. For ease of comparison, 5-year means were calculated and plotted in Figure 2.14 (thick lines). For all northern-hemisphere sectors, the time series of T_G show an increase in temperature starting around 1920/1930. This increase continues until about 1960 for all sectors except for Asia (blue curve), where the increase lasts for only ∼20 years. After a decrease in annual temperature in all 4 northern-hemisphere sectors starting in 1960 and lasting for about 10 years, a greater increase in temperature starting around 1970 and continuing until the end of the data set in 1996 can be observed. The 4 sectors of the southern hemisphere of T_G show a more steady increase in temperature from the beginning in 1860 until about 1960. After a decrease in annual temperature in the 1960s, temperature starts rising again from 1970 until the end of that data set in 1996.

The time series of T_{OF} in Figure 2.14 show that in the northern hemispheric sectors there is a relative high at about 1920 and a relative low at about 1935. A consistent increase in temperature from the 1930s can be seen in all 4 northern hemispheric sectors. The time series of the southern hemispheric sectors show no pronounced trend until about 1960 when temperatures in all 4 sectors accelerated significantly; in particular temperature increased from 0.003±0.002 K year^{-1} over 1921-1960 to 0.012±0.002 K year^{-1} over 1961-2000.

The drop in global temperature of T_G in the early 1960s, seen in all 8 sectors but particularly in the Pacific regions, are attributed to the volcanic eruption of

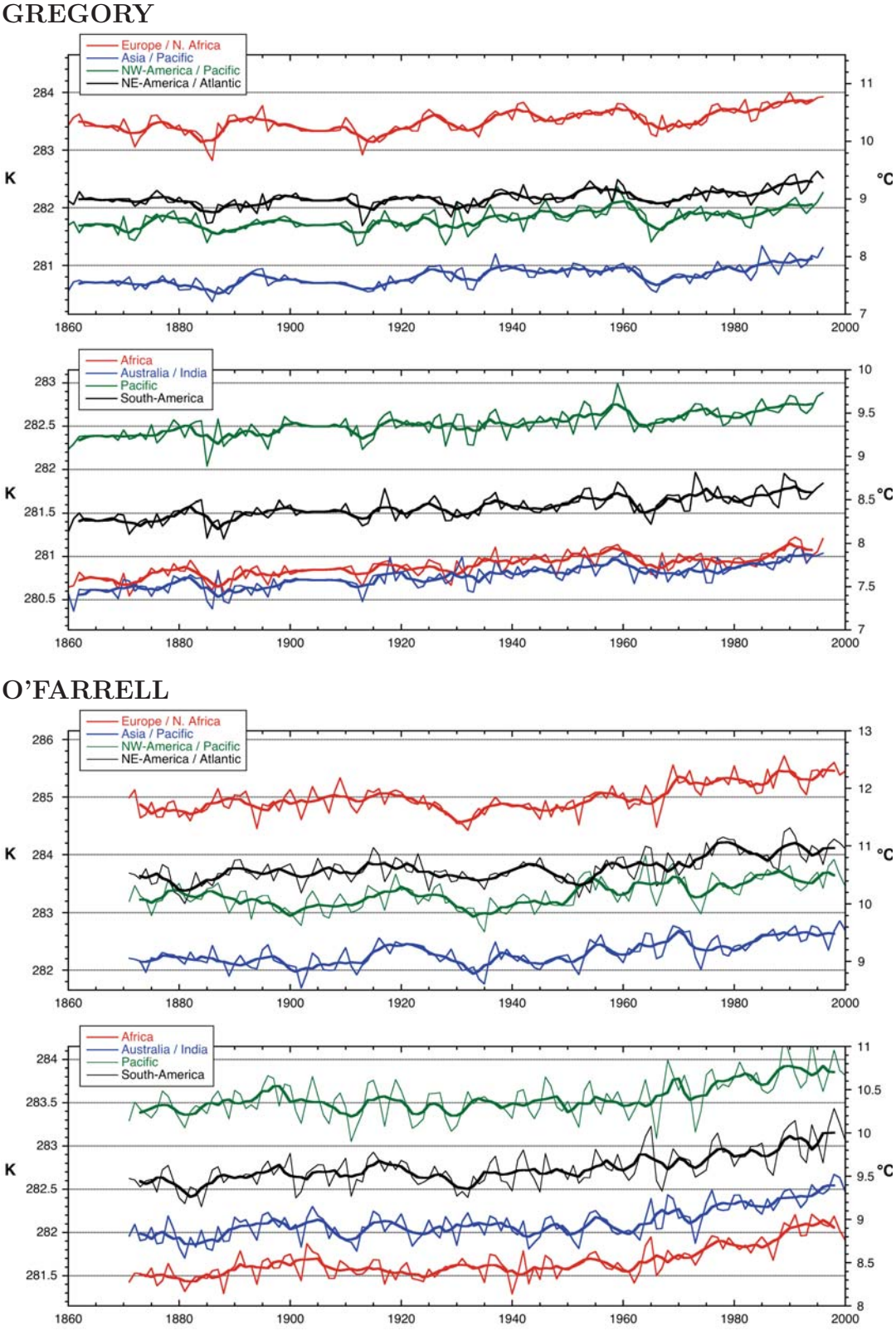

Figure 2.14: Time series of annual and 5-year mean (thick lines) surface atmospheric temperature in K provided by Gregory and O'Farrell of the northern and southern hemispheric sectors. For illustration purposes, temperature is also expressed in ^{o}C and plotted on the right axis. The different mean temperatures for the sectors can be explained by the fact that water bodies are generally warmer than land surfaces.

		1871-1990			1961-1990		
		ann	**sum**	**non-s**	**ann**	**sum**	**non-s**
GREGORY	**Northern hemisphere**						
	Europe / N. Africa	0.0032	0.0025	0.0035	0.0139	0.0145	0.0137
	20W-70E	±0.0004	±0.0004	±0.0005	±0.0032	±0.0034	±0.0030
	Asia / Pacific	0.0028	0.0010	0.0034	0.0118	0.0070	0.0135
	70E-160E	±0.0004	±0.0003	±0.0004	±0.0030	±0.0025	±0.0034
	NW-America/Pacific	0.0024	0.0018	0.0026	0.0064	0.0051	0.0068
	160E-250E	±0.0004	±0.0004	±0.0004	±0.0032	±0.0032	±0.0033
	NE-America/Atlantic	0.0019	0.0014	0.0020	0.0096	0.0120	0.0088
	250E-340E	±0.0003	±0.0004	±0.0004	±0.0020	±0.0027	±0.0021
	Southern hemisphere						
	S. Africa	0.0023	0.0021	0.0024	0.0039	0.0035	0.0041
	20W-70E	±0.0002	±0.0002	±0.0003	±0.0018	±0.0017	±0.0021
	Australia	0.0025	0.0021	0.0027	0.0050	0.0046	0.0051
	20W-70E	±0.0002	±0.0002	±0.0003	±0.0018	±0.0017	±0.0021
	Pacific	0.0025	0.0022	0.0026	0.0075	0.0047	0.0084
	160E-250E	±0.0003	±0.0003	±0.0003	±0.0017	±0.0016	±0.0019
	South America	0.0025	0.0021	0.0027	0.0071	0.0051	0.0078
	250E-340E	±0.0003	±0.0003	±0.0003	±0.0026	±0.0026	±0.0027
O'FARRELL	**Northern hemisphere**						
	Europe / N. Africa	0.0036	0.0033	0.0036	0.0178	0.0216	0.0165
	20W-70E	±0.0004	±0.0005	±0.0005	±0.0031	±0.0038	±0.0032
	Asia / Pacific	0.0031	0.0034	0.0030	0.0049	0.0051	0.0049
	70E-160E	±0.0004	±0.0004	±0.0004	±0.0026	±0.0027	±0.0028
	NW-America/Pacific	0.0030	0.0030	0.0030	0.0083	0.0051	0.0094
	160E-250E	±0.0005	±0.0004	±0.0005	±0.0037	±0.0036	±0.0039
	NE-America/Atlantic	0.0034	0.0035	0.0034	0.0146	0.0125	0.0152
	250E-340E	±0.0004	±0.0004	±0.0004	±0.0033	±0.0032	±0.0035
	Southern hemisphere						
	S. Africa	0.0027	0.0031	0.0026	0.0128	0.0139	0.0124
	20W-70E	±0.0002	±0.0002	±0.0003	±0.0018	±0.0018	±0.0019
	Australia	0.0027	0.0025	0.0027	0.0118	0.0117	0.0119
	70E-160E	±0.0003	±0.0003	±0.0003	±0.0019	±0.0023	±0.0020
	Pacific	0.0024	0.0023	0.0024	0.0159	0.0142	0.0165
	160E-250E	±0.0004	±0.0003	±0.0004	±0.0030	±0.0022	±0.0033
	South America	0.0028	0.0028	0.0028	0.0082	0.0070	0.0086
	250E-340E	±0.0003	±0.0004	±0.0003	±0.0028	±0.0032	±0.0029

Table 2.2: Division of the world into 8 global sectors. Linear trends and standards deviations (Equation 2.12) are calculated from annual (*ann*), summer (*sum*), and non-summer (*non-s*) modelled temperature data provided by Gregory and O'Farrell for the periods 1871-1990 and 1961-1990, expressed in K year^{-1}.

Mt. Agung (Bali) in 1963 (Newell, 1970). Three other major volcanic eruptions, Mount St. Helens in 1980, El Chichon (Mexico) in 1982, and Pinatubo (together with Cerro Hudson) in 1991 (Philippines), show a similar effect on the global temperature. However, these variations are shorter in duration and smaller in magnitude (see also Bradley, 1988; IPCC, 2001, Chapter 6.15). The decrease in temperature in each of the sectors as a result of the four volcanic eruptions mentioned above cannot be seen in the time series of T_{OF}; the reason for that being the lack of volcanic forcing in the T_{OF} model.

As a consequence of the independent model runs for the worlds temperature changes over the past decades and century, a constant bias of 1 to 1.5 K between the time series of the 8 sectors using T_G and T_{OF} can be observed. In particular, the model T_{OF} seems to run a slightly warmer climate than T_G.

Comparing the general pattern of temperature curves of T_G and T_{OF} in Figure 2.14 shows that the latter has less inter-annual variation but greater linear trends over time. Linear trends of the sectors' annual means (the standard deviation of the trends are calculated from Equation 2.12) for the period 1871-1990 listed in Table 2.2 are of the order of $0.002-0.003$ K year^{-1} for T_G. Temperature trends of T_{OF} of the 8 sectors are all consistently higher than those based on T_G by up to 0.0015 K year^{-1}. Again, this demonstrates the effect of two independent results of modelling global climate.

Trends for annual summer (June, July, and August for the northern hemisphere and December, January, and February for the southern hemisphere) and annual non-summer months (remaining months) are also listed in Table 2.2. In general, the non-summer months show mostly stronger positive trends than the trends of summer months and also than the annual trends. The consequences to this for mountain glaciers can be interpreted as less accumulation of snow and possibly more rainfall events during winter due to higher air temperatures. Additionally, a positive trend for summer months results in an increase in melting of glacier-ice. Summer and non-summer temperature trends of T_{OF} are also higher than those of T_G.

Compared to the temperature trends over the period 1871-1990, those calculated for 1961-1990 (listed in Table 2.2) are consistently higher in all 8 sectors, by a factor of up to 4, regardless of the data set used. The statement of consistently higher trends in T_{OF} compared to the trends in T_G for most of the 8 sectors is also valid for the period 1961-1990. Thus, it can be expected that these higher trends

in both the T_{OF} and within the more recent period 1961-1990 will also be reflected in the subsequent calculations of ice-volume changes of mountain glaciers.

2.3.4.2 Regional temperature variations

Another way of testing the reliability of the modelled temperature data set is to compare it with results of Oerlemans (2005). He analysed 169 glacier-length records in order to extract a climate signal. His reconstructions of the temperature for the different glacier-regions (Figure 3A in Oerlemans, 2005) from 1870 to 1990 show average changes in temperature of about

- $+0.0038$ K year^{-1} in Europe (Alps),
- $+0.0058$ K year^{-1} in Asia (Caucasus and Central Asia),
- $+0.0069$ K year^{-1} in the Southern Hemisphere (Tropics, New Zealand, and Patagonia),
- $+0.0010$ K year^{-1} in Northwest of America (mainly Canadian Rockies),
- $+0.0042$ K year^{-1} in the Atlantic (South Greenland, Iceland, Jan Mayen, Svalbard, and Scandinavia),

and a global[18] signal in temperature change of $+0.0057$ K year^{-1}. Consequently, a similar calculation for 8 regions using T_G and T_{OF} were undertaken for this study. The boxes in Figure 2.15 show the areas used for calculating regional mean temperature series, where both continent and ocean grid cells are used (no land mask is applied). Linear trends in temperature of both temperature data sets over the period 1871-1990 for the different regions are listed in Table 2.3.

As with the calculated temperature trends of the 8 sectors from the previous section, the regional temperature trends established from T_G are generally lower than those obtained using T_{OF} (Table 2.3). Linear trends of the regions Asia, Patagonia, and South America have relatively high values, consistent with the results found for Asia and the Southern Hemisphere in Oerlemans (2005). The small trend in NW-America determined by Oerlemans (2005) can only be reproduced with T_G. The linear trend in temperature in Europe determined by Oerlemans (2005) is larger than from the calculation using either of the two temperature data sets. Overall comparison shows differences in the two temperature data sets themselves, i.e. in a few regions the error bars do not overlap.

[18] Oerlemans (2005) calculated this global signal based on the temperature trends of the five regions by weighting them accordingly: 0.5 for the Southern Hemisphere, 0.1 for Northwest America, 0.15 for the Atlantic sector , 0.1 for the Alps and 0.15 for Asia

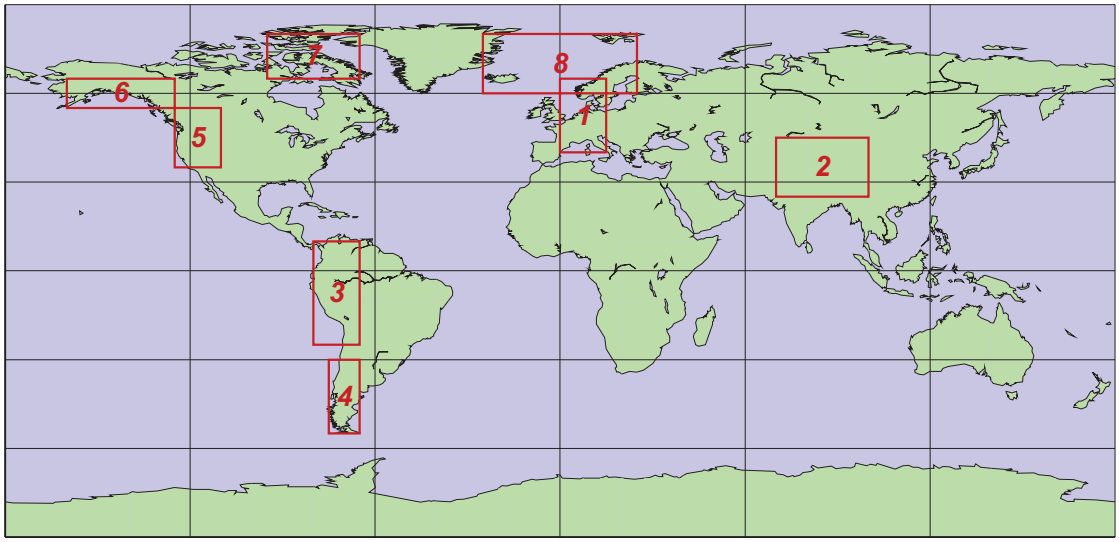

Figure 2.15: Boxes indicate the extent of regions for which regional temperature trends have been calculated.

The global temperature change derived from glacier records by Oerlemans (2005) of 0.0057 K year^{-1} over the period 1870-1990 is greater than that of T_G and T_{OF}. The relatively high global trend is unsurprising as the high temperature trend obtained for the Southern Hemisphere region (Tropics, New Zealand, and Patagonia) of 0.0069 K year^{-1} is representative for half the globe (Oerlemans, 2005, applied a weighting factor of 0.5). If a similar 'weighting-exercise' is undertaken here (i.e. weighting the trends of similar regions by the same factors as in Oerlemans (2005): 0.1 for Europe, 0.15 for Asia, 0.5 for South America plus Patagonia, 0.1 for NW-America plus Alaska, 0.15 for the Arctic[19]) using the regional trends of T_G and T_{OF} results in estimates for the global temperature change of ∼0.0036 and ∼0.0046 K year^{-1}, respectively, both numbers lower than that obtained by Oerlemans (2005). As data of T_G and T_{OF} are available globally the corresponding global temperature trends are calculated to 0.0025±0.0002 and 0.0030±0.0004 K year^{-1}, respectively, which are only about half the estimate of Oerlemans (2005).

Although these modelled trends are strongly dependent on the chosen size and locations of the regions (boxes in Figure 2.15) and therefore vary correspondingly, generally a good agreement of regional trends in temperature between different approaches can be observed. Also, the statement of great variability in temperature changes around the world is confirmed with both temperature data sets, T_G and T_{OF}.

[19]note that, like in Oerlemans (2005), I have not included NE-America

	Region	Latitude	Longitude	trend	
				Gregory	O'Farrell
1	**Europe**	40N - 65N	0E - 15E	0.0018±0.0010	0.0023±0.0009
2	**Asia**	25N - 45N	70E - 100E	0.0038±0.0009	0.0058±0.0010
3	**South America**	25S - 10N	280E - 295E	0.0054±0.0013	0.0073±0.0024
4	**Patagonia**	55S - 30S	285E - 295E	0.0032±0.0007	0.0035±0.0007
5	**NW-America**	35N - 55N	235E - 250E	0.0012±0.0011	0.0044±0.0012
6	**Alaska**	55N - 65N	200E - 235E	0.0024±0.0012	0.0010±0.0014
7	**NE-America**	65N - 80N	265E - 295E	0.0001±0.0007	0.0037±0.0010
8	**Arctic**	60N - 80N	25W - 25E	0.0036±0.0009	0.0033±0.0009
	global			0.0025±0.0002	0.0030±0.0004

Table 2.3: Regions determined for the calculation of linear temperature trends (standards deviation computed from Equation 2.12) over the period 1871-1990 expressed in K year^{-1}. A comparison of results between temperature data sets of Gregory and O'Farrell is given.

2.3.4.3 Correlation with observed temperature data

In order to check the reliability of the modelled temperature data sets of Gregory and O'Farrell, time series for several glaciated regions have been compared with observed temperature series at sites where the latter is available. These observed temperature series have been taken from the NASA web page[20]. The NASA GISS Surface Temperature (GISTEMP) provides a measure of the changing global surface temperature with monthly resolution since 1880.

Correlation coefficients between time series of T_G and observed temperature are listed in Table B.5 on page 316 and are relatively low in many regions. In remote areas, like the Alaskan Peninsula and glaciated regions at the South Indian Islands, in Papua New Guinea, in Mexico and in some parts of Patagonia, correlation coefficients are close to zero. Except for Patagonia, these glaciated regions cover a relatively small area and contribute little to the global change in mass balance. Correlation coefficients of only 0.15 are calculated for Svalbard and Franz-Josef Land. Central Asia shows correlation coefficients of up to 0.5. Parts of the regions in North-West America also show low correlation coefficients. Some correlation coefficients in Alaska are relatively high (up to 0.5), whereas those in the European Alps are lower (up to 0.3). Correlation coefficients of T_{OF} and observed temperature time series are listed in Table B.6 on page 317 and indicate similar results as above, i.e. the correlation coefficients seem to be low, mostly not exceeding 0.3.

[20] http://www.giss.nasa.gov/data/update/gistemp/station_data

Other than uncertainties in the modelled temperature data sets, reasons for low correlation coefficients may also be that in the regions of interest, the observed temperature might not be available from nearby stations and the correlations are based on data from stations that are further away. Moreover, the stations of the GISS TEMP data base are mostly located in or near populated regions (cities, airports, coastal areas, etc.) but where possible stations in rural areas were chosen in order to avoid any influences coming from the populated regions. Although temperature observations from high altitude weather stations can be very valuable for estimating the temperature conditions over nearby glaciers it is also possible that the climate at a weather stations is decoupled from the climatic conditions at the glacier (see also Section 2.2.1; Oerlemans, 2001). Hence, the low degree of correlation might be due to these reasons, rather than the mismatch between modelled data and the climate at the glaciated region.

2.3.4.4 Temperature anomalies

In order to calculate ice-volume changes of mountain glaciers, Zuo and Oerlemans (1997a) used an observed temperature data set. They determined the required temperature time series by using data from stations, many of which are quite distant from the glaciated region (see boxes in Figure 2.16). The average temperature of all stations within a box represents the climate for all glaciated regions (red stars) located within that box. Consequently, when using the observed temperature data set, the climate of 100 glaciated regions are represented by temperature time series of 34 boxes, some of which are quite large.

In this thesis, the two modelled temperature data sets provided by Gregory and O'Farrell are used. One reason for this choice is that despite several attempts it has not been possible to reproduce the results of Zuo and Oerlemans (1997a) using an observed temperature data set. Another disadvantage of using the observed data set is the large time gaps in the observational records especially before 1900. From the modelled data of T_G and T_{OF}, time series for each of the 100 glaciated regions can be estimated from the temperature in the nearest grid cell. This approach avoids averaging over large areas and therefore likely provides a better link between the glaciated region and its climate.

To calculate temperature anomalies (required parameter for Equation 2.3) from the time series, the following steps have been applied, although step 1 is only necessary for T_G:

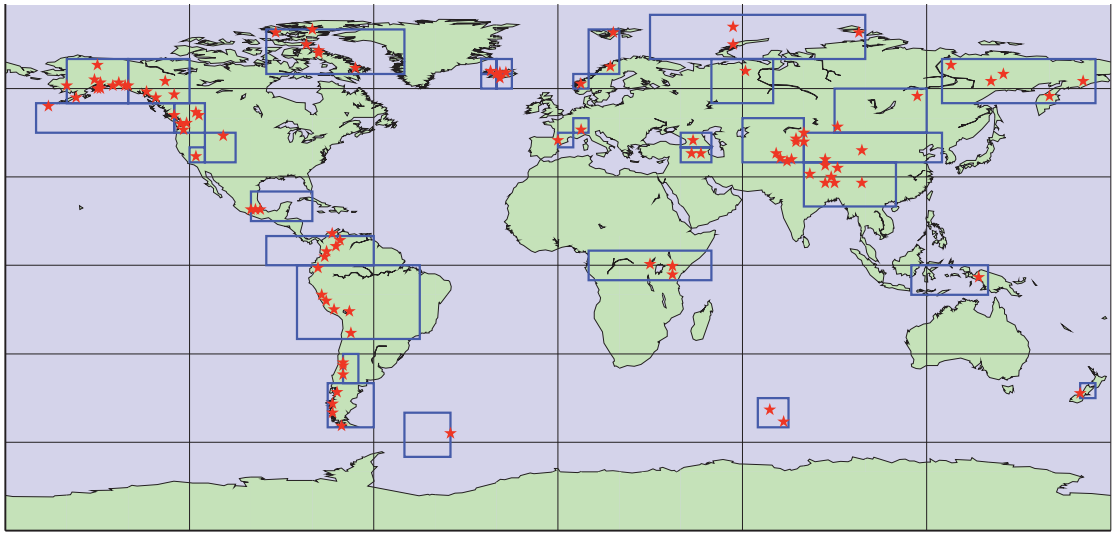

Figure 2.16: Locations of 100 glaciated regions (red stars) of Zuo and Oerlemans (1997a). Blue boxes indicate the areas where observed temperature data have been averaged by Zuo and Oerlemans (1997a) in order to obtain time series for the glaciated regions within the box.

1. **Completion of temperature data set**

   The modelled temperature data set provided by Gregory is not complete, with data for 212 months (13% of total) missing due to problems of data recovery from the Hadley Centre computer runs. To interpolate for the missing months, mean monthly temperature over periods of about 20 years approximately centred on the missing data have been calculated (see last column in Table 2.4). These are used to fill the gaps in the existing data set.

missing months	amount	time periods for interpolation
1862/09 to 1862/09	1	1860 / 01 - 1879 / 12
1863/01 to 1868/08	68	
1868/12 to 1868/12	1	
1892/06 to 1892/08	3	1880 / 01 - 1899 / 12
1901/10 to 1909/11	98	1900 / 01 - 1924 / 12
1921/09 to 1923/05	21	
1979/12 to 1981/07	20	1970 / 01 - 1989 / 12
total	212	

Table 2.4: List of missing months of modelled temperature data set provided by Gregory. The last column lists the time periods used for the interpolation to fill missing months.

2. **Annual summer and annual non-summer temperature series**

   Gridded monthly temperatures are now available for the entire period from 1860-1996 and 1871-2000 for both temperature data sets. The annual summer temperatures $T_{s,k}$ is defined as

$T_{s,k}$ = annual mean of June/July/August for the northern hemisphere, and December/January/February for the southern hemisphere, respectively.

The annual non-summer temperature $T_{ns,k}$ is defined as

$T_{ns,k}$ = annual mean of remaining months.

These time series have been calculated for each glaciated region k.

3. **Reference periods**
In order to calculate the glacier melt, according to Equation 2.3, temperature anomalies relative to the climate state for the period before 1900 are required. This reference period should be a time where the climate is in equilibrium with the extent of the glaciated regions, i.e. the glacier is in steady state, not changing in volume on an annual time scale. The reference period can be interpreted as a time without any climatic changes. Reference annual summer $T_{ref,s,k}$ and reference annual non-summer $T_{ref,ns,k}$ temperatures for each glaciated region k have been determined by calculating the mean temperature over the corresponding years.

$T_{ref,s,k}$ = mean of $T_{s,k}$ for years within the reference period
$T_{ref,ns,k}$ = mean of $T_{ns,k}$ for years within the reference period

Figure 2.17 shows temperature averages for both hemispheres and a global one based on observations calculated by Jones et al. (1999). There is an obvious increase in temperature at the beginning of the 20^{th} century, and it is important to select a reference period before the onset of warming (red highlighted area in the figure). In the large scale temperature variations of Figure 2.14 the onset of warming at ∼1900 is not easy to identify, however, expressed in numbers, the global trend (in T_{OF}) over the period 1871-1895 of 0.028 K year^{-1} increases to 0.0051 K year^{-1} during 1901-1925.

Several reference periods have been selected in order to establish whether their choice is critical and whether an optimum period can be identified. Since data of T_G is missing for a time span of more than 5 years in the mid 1860s, it is reasonable to use a reference period starting in 1866 or later in order to avoid the full integration of the interpolated years into the calculation. Furthermore, since temperature data of T_{OF} is only available from 1871 onwards, all further calculations will start with the year 1871 unless specified differently. Finally, the reference period 1871-1895 is chosen to stay well outside the period where global warming commenced (around 1900).

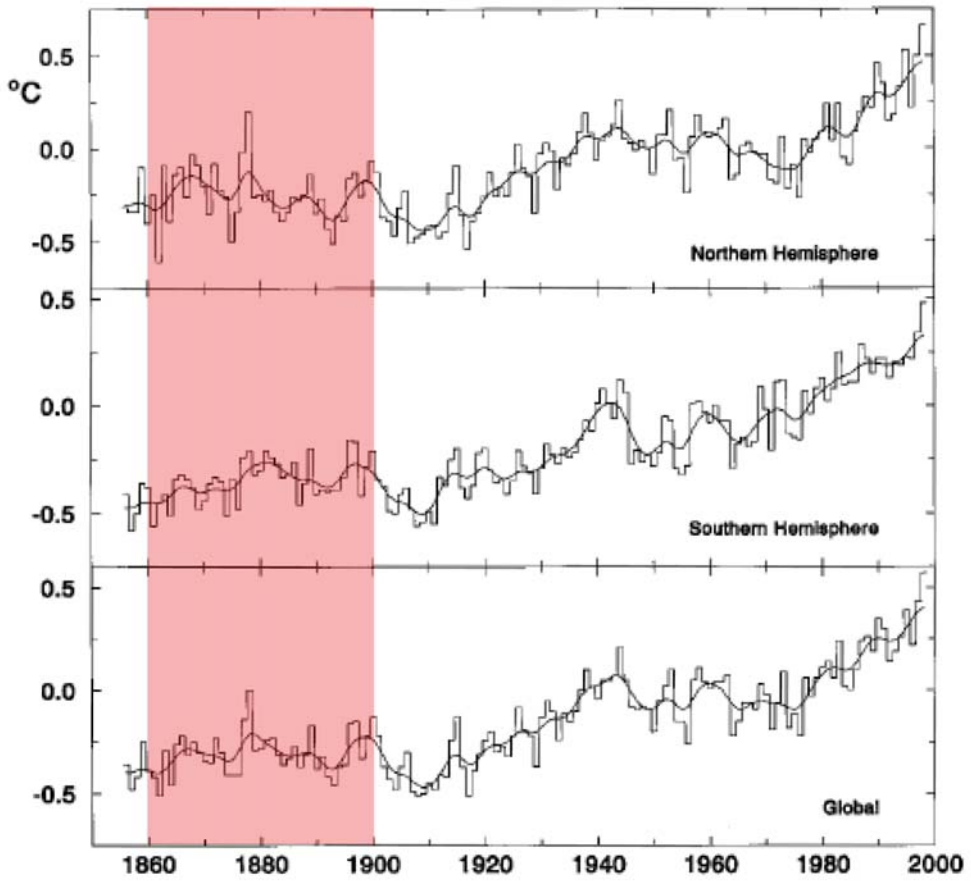

Figure 2.17: Hemispheric and global temperature averages determined by Jones et al. (1999) starting in 1854 and relative to 1961-1990. The red highlighted area illustrates the time within which the reference period should be defined.

4. **Temperature anomalies**

   Finally, temperature anomalies for the entire period (e.g. 1871-1990) have been obtained by subtracting the reference temperature obtained for the period 1871-1895 from the annual summer and annual non-summer temperature. This has been done for each glaciated region k.

$$\Delta T_{s,k} = T_{s,k} - T_{ref,s,k}$$
$$\Delta T_{ns,k} = T_{ns,k} - T_{ref,ns,k}$$

   With this final step the temperature anomalies required in Equation 2.3 are now available. Note that using temperature anomalies (and not absolute temperatures) has the advantage that corrections of the modelled temperature due to different altitudes of glaciers are not necessary.

2.3.5 Glacier imbalance and climate state

Section 2.2 presented evidence for the imbalance between glacier and climate state before 1900, with case studies of observed glacier changes. All these studies indicate that the glaciers were still responding to recent past or prevailing climatic changes. In general, the extent of these glaciers reflected a slightly cooler climate. This fact is accounted for by introducing the correcting factor Θ in Equation 2.3. The parameter Θ can be defined as the difference between the current temperature and the temperature with which the current glacier volume is in equilibrium. In Section 2.2 one means of quantifying this parameter using observed glacier length records and sensitivity models is presented. From these studies the parameter Θ would be set to between 0.10 and 0.15 K. Zuo and Oerlemans (1997a) introduced three different values for Θ: 0.00, -0.15, and -0.30 K[21] and concluded that the middle value gives the best estimate of global ice-volume change (i.e. they apply this parameter globally). However, this imbalance of glacier and climate state is unlikely to be globally uniform, as will be discussed in the following three sections.

Another approach to determining the parameter Θ using the modelled temperature data sets T_G and T_{OF} involves calculating the temperature change over a period corresponding to the response time of glaciers to recent temperature changes. The assumption is made in this thesis that the response time of glaciers is 25 years. This is, of course, only a very rough estimate, as the response time of glaciers depends on many factors, including the geometry of the glacier and the change in ice-volume (e.g. Harrison et al., 2001), and therefore varies from glacier to glacier. According to Jóhannesson et al. (1989), a glacier with a thickness of 200 m and a mass balance rate of -10 m year^{-1} has a response time of 50 years. However, worldwide many glaciers are smaller in their sizes than the one mentioned above and therefore a shorter response time of 25 years is chosen for this thesis. Another assumption that has to be made here is that the temperature trend prior 1871 is the same as the one over the period 1871-1895. This is because the imbalance between glacier and climate state is calculated over the period 1871-1895 but actually is caused by the delayed response of climatic changes (i.e. temperature changes) prior to 1871. In the following three sections different approaches of estimating the imbalance Θ between glacier and climate state are presented, while all of them are based on the temperature change over the period 1871-1895.

[21] as noted previously, unlike in the study of Zuo and Oerlemans (1997a), Θ is applied positive in this thesis

2.3.5.1 Large scale temperature variations within the reference period

Using modelled data sets for calculating linear trends in annual temperature for the 8 global sectors during 1871-1895 (see Table 2.5) results partly in negative trends for sectors in both hemispheres using T_G. However, this cooling is never statistically significant at a 2σ level. A decrease in observed temperature over the same period in Figure 2.17 of Jones et al. (1999) can be, if at all, observed in the northern hemisphere only. Other evidence for temperature changes, in particular observations of global glacier retreat before 1900 discussed in Section 2.2, do not indicate a cooling climate. Since changes in glaciers are likely to be a result of both variations in summer and non-summer temperature, those have been also listed in Table 2.5. Some of the linear trends in summer and non-summer temperatures of T_G over the period 1871-1895 of the 8 sectors are negative but again never statistically significant at a 2σ level.

When assessing the annual temperature trends of the 8 sectors for the reference period 1871-1895 using T_{OF}, similar conclusions as for T_G can be drawn. Most of the trends in the sectors of the southern hemisphere are higher compared to those using T_G. However, none of the annual trends of both hemispheric sectors are statistically significant at a 2σ level.

The results of T_G and T_{OF} also show that the temperature trends within the reference period are not the same, even on very large scales. Although, the two temperature data sets have different trends in all sectors, partly also with the opposite sign, most of the error bars overlap. On a global scale, using the trends in T_G and T_{OF} within the reference period of 0.0014 and 0.0028 K year^{-1}, respectively, results in a total temperature change of 0.04 and 0.07 K, respectively, over the 25-year period.

2.3.5.2 Individual temperature variations of 100 glaciated regions within the reference period

Linear trends in temperature of the 100 glaciated regions using the nearest grid point of T_G range from -0.075 to $+0.161$ K year^{-1}. The histograms in Figure 2.18 show that T_{OF} clearly produces more positive trends in temperature over the period 1871-1895 for the same 100 glaciated regions than T_G. Annual trends of T_{OF} range from -0.019 to $+0.259$ K year^{-1}. A comparison of the linear trends of the 100 glaciated regions for T_G and T_{OF} is listed in Table B.8 on page 321. Whereas 59 of

			annual	summer	non-summer
GREGORY	**Northern hemisphere**				
	Europe / N. Africa	20W - 70E	0.0100	−0.0004	0.0135
			±0.0059	±0.0049	±0.0063
	Asia / Pacific	70E - 160E	0.0044	0.0009	0.0056
			±0.0039	±0.0041	±0.0043
	NW-America / Pacific	160E - 250E	−0.0016	0.0027	−0.0031
			±0.0043	±0.0034	±0.0047
	NE-America / Atlantic	250E - 340E	−0.0058	−0.0066	−0.0055
			±0.0036	±0.0038	±0.0039
	Southern hemisphere				
	S. Africa	20W - 70E	0.0018	0.0018	0.0018
			±0.0031	±0.0027	±0.0034
	Australia	70E - 160E	−0.0022	0.0040	−0.0043
			±0.0031	±0.0034	±0.0033
	Pacific	160E - 250E	0.0002	0.0014	−0.0002
			±0.0035	±0.0035	±0.0037
	South America	250E - 340E	0.0044	0.0076	0.0033
			±0.0032	±0.0035	±0.0032
O'FARRELL	**Northern hemisphere**				
	Europe / N. Africa	20W - 70E	0.0024	−0.0042	0.0045
			±0.0051	±0.0050	±0.0056
	Asia / Pacific	70E - 160E	−0.0023	−0.0025	−0.0022
			±0.0034	±0.0038	±0.0042
	NW-America / Pacific	160E - 250E	−0.0023	−0.0039	−0.0024
			±0.0048	±0.0040	±0.0053
	NE-America / Atlantic	250E - 340E	0.0052	0.0008	0.0066
			±0.0051	±0.0049	±0.0054
	Southern hemisphere				
	S. Africa	20W - 70E	0.0048	0.0026	0.0056
			±0.0030	±0.0024	±0.0034
	Australia	70E - 160E	0.0045	0.0024	0.0033
			±0.0038	±0.0046	±0.0039
	Pacific	160E - 250E	0.0063	0.0046	0.0058
			±0.0032	±0.0028	±0.0036
	South America	250E - 340E	0.0035	−0.0013	0.0051
			±0.0035	±0.0041	±0.0038

Table 2.5: Linear trends including standards deviations (from Equation 2.12) of *annual*, *summer*, and *non-summer* temperature in K year^{-1} of 8 global sectors for the period 1871-1895. The temperature data set of Gregory and O'Farrell are used.

the annual trends in the 100 glaciated regions using T_G are negative, only three of them are statistically significant at a 2σ level. Of the 41 positive temperature trends only five are statistically significant at the same confidence level. When using T_{OF} none of the 18 glaciated regions with a negative sign are statistically significant at a 2σ level. However, of all regions with a positive trend in temperature when using T_{OF}, 15 are statistically significant at a 2σ level.

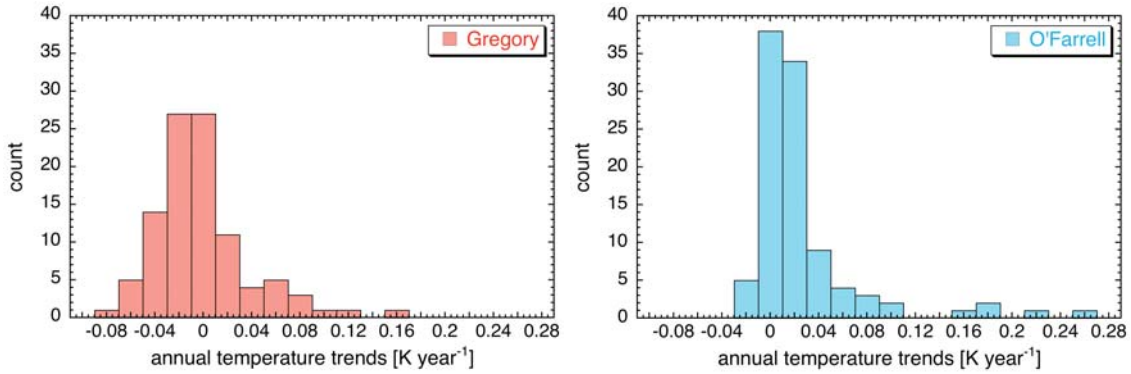

Figure 2.18: Histogram of linear trends in annual temperature in K year^{-1} over the period 1871-1895 of 100 glaciated regions of the Gregory and O'Farrell temperature data sets.

In conclusion, the individual temperature trends indicate that there was a disequilibrium between the climate and the glacier state within the reference period. The degree of imbalance varies significantly in magnitude from region to region, and ominously, depending on the temperature data set used. Calculating the area-weighted mean of all 100 individual trends of T_G gives a value of -0.0062 ± 0.0030 K year^{-1}, only slightly different from zero. However, using T_{OF} results in a weighted mean of $+0.0293\pm0.0260$ K year^{-1}. For the 25-year period this corresponds to a change in temperature of -0.16 and $+0.73$ K, respectively.

2.3.5.3 Regional temperature variations within the reference period

Another way of quantifying the parameter Θ is to calculate regional trends over areas of a few tens of degrees square. The boundaries of 8 regions are listed in Table 2.6 and are also shown as boxes in Figure 2.15 on page 52. Linear trends in annual temperature of these regions for the period 1871-1895 include negative signs but none of these negative trends are statistically significant at a 2σ level (Table 2.6). Temperature trends for most of the 8 regions using T_{OF} are positive and higher compared to those of T_G. For some regions, the temperature trends are statistically significant at a 2σ level. Again, these results are consistent with

the various trends calculated previously at both smaller and larger scales. The calculated trend over the areas [1-6] using T_{OF} of 0.0096±0.0038 K year^{-1} lies within the global estimate of Oerlemans (2005) of ∼0.006 K year^{-1} derived over the period 1860-1890 (Figure 3A in Oerlemans, 2005). The global result of Oerlemans (2005) also agrees with the calculated trend of all 8 regions when using T_{OF} (see last row in Table 2.6).

With the regional trends of Table 2.6, the parameter Θ can be now quantified for the 8 regions over a 25-year period, i.e. from the two temperature data sets estimates for Θ are listed in Table 2.7. Global estimates for Θ derived by combining all 8 regions when using T_G and T_{OF} are −0.013±0.095 and 0.150±0.060 K, respectively, provided the same 25-year reference period is used. The latter result complements the Θ value proposed by Zuo and Oerlemans (1997a).

	Region	Lat.	Long.	trend	
				Gregory	O'Farrell
1	**Europe**	40N - 65N	0E - 15E	0.0150±0.0109	0.0256±0.0055
2	**Asia**	25N - 45N	70E - 100E	−0.0075±0.0107	0.0133±0.0065
3	**South America**	25S - 10N	280E - 295E	0.0139±0.0156	0.0062±0.0138
4	**Patagonia**	55S - 30S	285E - 295E	−0.0002±0.0073	−0.0016±0.0046
5	**NW-America**	35N - 55N	235E - 250E	−0.0120±0.0140	−0.0021±0.0096
6	**Alaska**	55N - 65N	200E - 235E	−0.0207±0.0106	0.0062±0.0087
7	**NE-America**	65N - 80N	265E - 295E	−0.0129±0.0090	0.0151±0.0084
8	**Arctic**	60N - 80N	25W - 25E	0.0276±0.0082	0.0339±0.0057
	areas [1−6]			−0.0009±0.0063	0.0096±0.0038
	areas [1−8]			−0.0005±0.0038	0.0060±0.0024

Table 2.6: Linear trends including standards deviations (from Equation 2.12) in annual temperature in K year^{-1} of 8 different regions for the period 1871-1895 of the Gregory and O'Farrell temperature data sets.

	Region	Latitude	Longitude	Θ	
				Gregory	O'Farrell
1	**Europe**	40N - 65N	0E - 15E	0.38	0.64
2	**Asia**	25N - 45N	70E - 100E	−0.19	0.33
3	**South America**	25S - 10N	280E - 295E	0.35	0.15
4	**Patagonia**	55S - 30S	285E - 295E	−0.01	−0.04
5	**NW-America**	35N - 55N	235E - 250E	−0.30	−0.05
6	**Alaska**	55N - 65N	200E - 235E	−0.52	0.16
7	**NE-America**	65N - 80N	265E - 295E	−0.32	0.38
8	**Arctic**	60N - 80N	25W - 25E	0.69	0.85
	areas [1−8]			−0.013	0.150

Table 2.7: Parameter Θ listed for 8 different regions determined from the temperature changes over the period 1871-1895 based on the Gregory and O'Farrell temperature data sets.

The following distribution of glaciers within the 8 regions is used to calculated a differently weighted global value: Asia, Alaska, and Arctic contain each 20% of the total glacier area, Europe and South America each 1%, NE-America 28%, Patagonia 6%, and NW-America 4%. Subsequently, from the two temperature data sets, global estimates for the parameter Θ are -0.24 and 0.35 K.

Summarising, it is not easy to find satisfying results for the parameter Θ. Different temperature data sets result partly in significantly different estimates for Θ on a global, individual, and regional scale (sometimes even with opposite signs). However, T_{OF} produces global estimates which are closer to the observational value used by Zuo and Oerlemans (1997a) than those in T_G. Also, regional and large scale estimates of Θ derived from T_{OF} are in general more comparable to other observations (e.g. Section 2.2).

2.4 Summary

In this chapter observational and numerical approaches used to estimate ice-volume changes in mountain glaciers have been presented and assessed. Observational data on mass balances is only available for a few glaciers (Dyurgerov and Meier, 2005) and the observed time intervals are not always continuous. In contrast, a numerical approach has the advantage that an estimate can be calculated globally and continuously over time (provided that global data sets are available). In particular, a seasonally and regionally differentiated approach based on a few parameters has been introduced. The numerical methods have, however, their own limitations in that they do not reflect all the processes that contribute to the mass balance change. Additionally, the available model parameters (particularly precipitation and temperature) may not reflect the conditions at the glacier surface. Therefore, the global data sets required for the numerical approach have been discussed in detail and where possible compared with observational data. From this assessment of the various temperature and precipitation data sets, however, it was not possible to explicitly single out a superior model and hence each of the data sets introduced here are used in the following chapter.

In the numerical model of mountain deglaciation, a further parameter Θ accounting for the initial imbalance of glacier and climate state has been introduced. This parameter varies greatly from region to region and is also dependent on whether it is derived from observations or numerically. If the latter is the case, subsequently

the data set used also affects the estimates for the parameter Θ. When attempting to apply this parameter globally, it is difficult to isolate with confidence a single representative number. Therefore, if Θ is applied globally in this thesis it is set to 0.15 K (as suggested by Zuo and Oerlemans, 1997a), unless otherwise specified. Additionally, regionally variable values for Θ are used and thus the effect on the results compared to a global value are assessed in the following chapter.